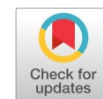


Available online at [www.synsint.com](http://www.synsint.com)

# Synthesis and Sintering

ISSN 2564-0186 (Print), ISSN 2564-0194 (Online)



## Review article

# New updates on vanadate compounds synthesis and visible-light-driven photocatalytic applications

Mehrdad Mirzaei <sup>a,\*</sup>, Asieh Akhoondi <sup>b,\*</sup>, Wael Hamd <sup>c</sup>, Jorge Noé Díaz de León <sup>d</sup>, Rengaraj Selvaraj <sup>e</sup>

<sup>a</sup> Nanomaterials Group, Department of Materials Engineering, Tarbiat Modares University, P.O. Box 14115-143, Tehran, Iran

<sup>b</sup> Department of Chemical Engineering, Arak Branch, Islamic Azad University, Arak, Iran

<sup>c</sup> Chemical Engineering Department, Faculty of Engineering, University of Balamand, P.O. Box 33, El-Koura, Lebanon

<sup>d</sup> Universidad Nacional Autónoma de México, Centro de Nanociencias y Nanotecnología, Km. 107, C. P. 22800, Ensenada, Baja California, México

<sup>e</sup> Department of Chemistry, College of Science, Sultan Qaboos University, P.O. Box- 36, P.C. 9 123, Al-Khoudh, Muscat, Oman

## ABSTRACT

Photocatalysis is known as a new and cost-effective method to solve the problems of energy shortage and environmental pollution. Although the application of this method seems practical, finding an efficient and stable photocatalyst with a suitable bandgap and visible-light sensitivity remains challenging. In this context, vanadate compounds photocatalysts have been synthesized and used as emerging composites, and their efficiency has been improved through elemental doping and morphology modifications. In this review, the major synthesis methods, and the design of the latest photocatalytic compounds based on vanadate are presented. In addition, the effect of vanadate microstructures on various photocatalytic applications such as hydrogen production, CO<sub>2</sub> reduction, and removal of organic pollutants and heavy metals are discussed. For instance, the application of a 2D-1D BiVO<sub>4</sub>/CdS heterostructure photocatalyst enhances 40 times the hydrogen production from benzyl alcohol than pure BiVO<sub>4</sub>. Similarly, the InVO<sub>4</sub>/Bi<sub>2</sub>WO<sub>6</sub> composite has a superior photocatalytic capability for the reduction of CO<sub>2</sub> into CO compared to pure InVO<sub>4</sub>. A CO production rate of 18 μmol.g<sup>-1</sup>.h<sup>-1</sup> can be achieved by using this heterostructure. Regarding the organic pollutants' removal, the use of Montmorillonite/BiVO<sub>4</sub> structure allows a complete removal of Brilliant Red 80 dye after only 2 hours of irradiation. Finally, copper heavy metal is reduced to 90% in water, by using BiVO<sub>4</sub>/rGO/g-C<sub>3</sub>N<sub>4</sub> optimized photocatalyst structure. Other examples on decorated vanadate compounds for enhancing photocatalytic activities are also treated.

© 2023 The Authors. Published by Synt Research Group.

## KEYWORDS

Photocatalyst  
Synthesis  
Solar energy  
Vanadate compound  
Nanocomposite



## 1. Introduction

The increase in industrial contaminants and global energy demand have encouraged the development of new green technologies as an alternative to fossil fuels and non-renewable resources in developed countries. [1, 2]. Solar energy as a cheap, unlimited, and pollution-free

source of irradiation has a clear perspective of photocatalysis [3]. However, the low irradiation energy of sunlight is a clear obstacle in the case of high band energy semiconductors. [4]. Hence, research efforts have been devoted to ameliorating photocatalysts' efficiency by modifying their microstructure and band gap energy allowing maximum absorption of a wide range of sunlight spectrum.

\* Corresponding author. E-mail address: [mehrdad.mirzaei@modares.ac.ir](mailto:mehrdad.mirzaei@modares.ac.ir) (M. Mirzaei), [asieh.akhoondi@gmail.com](mailto:asieh.akhoondi@gmail.com) (A. Akhoondi)

Received 4 December 2022; Received in revised form 28 March 2023; Accepted 29 March 2023.

Peer review under responsibility of Synt Research Group. This is an open access article under the CC BY license (<https://creativecommons.org/licenses/by/4.0/>).  
<https://doi.org/10.53063/synsint.2023.31132>

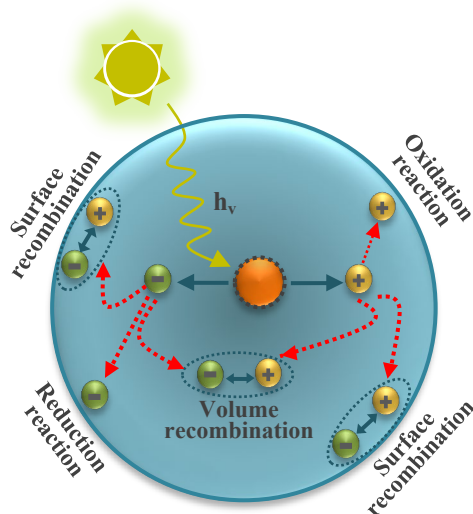


Fig. 1. Schematic fundamentals of photocatalysis in heterogeneous semiconductor.

In general, photocatalysts are wide bandgap semiconductors that could participate in redox reactions with light absorption and have many applications, including hydrogen production through water splitting [5–7], wastewater treatment, and removing pollutants such as dyes, drugs, and cosmetics [8–10].

In the previous paper that was published in 2021, a detailed report on the design and fabrication of vanadium compounds for photocatalytic uses under visible light was prepared [11]. During the last two years, extensive research has been done on this category of composites, which requires serious focus to advance future experiments. Therefore, in the upcoming review, the latest photocatalytic achievements of this popular group of materials are presented.

## 2. Basic properties of photocatalysts

Understanding the photocatalysis processes allows tuning the desired properties of the photocatalyst [12]. In this direction, three critical steps take place in this process, which occurs in all types of photocatalytic applications [13]: 1) photoexcitation and creation of electron-hole pairs, 2) transfer of photogenerated carriers to the surface, and 3) occurrence of photocatalytic reactions (Fig. 1). Photons that have more energy than the bandgap are absorbed by the semiconductor composite and cause the excitation of electrons from the valence band and the creation of positively charged holes. The photogenerated charges are transferred to the semiconductor surface during interactions and participate in photocatalytic reactions. Therefore, the characteristics of a suitable semiconductor as a photocatalyst are determined based on the three following steps [14]. i) Adequate bandgap width, ii) ability to absorb photons, and iii) sensitivity to a wide range of light irradiation. Hence, the ability to catalyze light-driven reactions is linked to the efficiency of electron-hole pair production and swift carrier transfer within the photocatalysts made from composite materials when exposed to visible light. In addition, nontoxicity and recyclability are noteworthy properties necessary for photocatalysts' reusability. The nanostructure of the photocatalyst must be such that it absorbs the photoproduced electrons and prevents the recombination of charge carriers in order to increase the quantum efficiency [15].

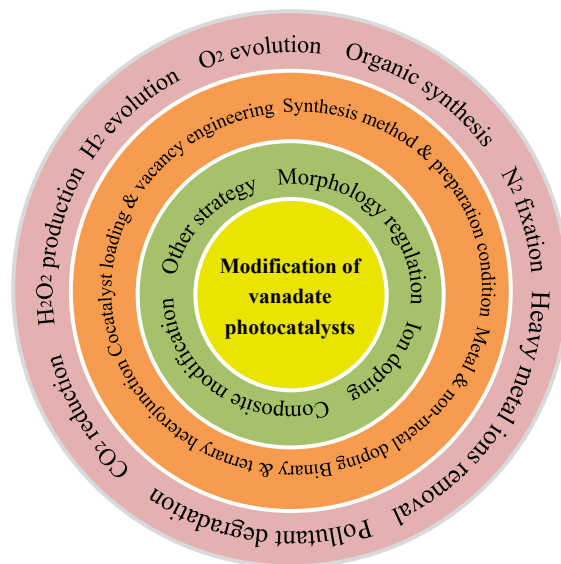


Fig. 2. Schematic strategy for modification of vanadate photocatalysts.

## 3. Synthesis and design of vanadate compounds

The type of material preparation method has a significant effect on the physicochemical properties and photocatalytic efficiency [16]. Therefore, its structural features are highly dependent on the selection of the synthesis method and its conditions. Various techniques have been utilized to enhance photocatalytic performance. The morphology, particle size, and crystallinity of semiconductors have a direct relationship with their photocatalytic activity because most of the photocatalytic reactions are performed on the surface of the composite. Until now, different approaches of vanadate photocatalysts especially contain modification of morphology, facet engineering, metal and non-metal doped strategy, hierarchical microstructures, and binary composites fabrication, among others (as shown in Fig. 2) to increase the available area for reactions and facilitate the separation of photogenerated charge carriers [17]. On the other hand, it is clear that particle size, crystallinity, specific surface area, and grain morphology that depend on the preparation method and conditions, often largely determine the physicochemical properties of nanomaterials and micro-materials [18]. Many technologies have been represented for photocatalyst syntheses such as the hydro/solvothermal route, sol-gel method, flame spray synthesis method, and co-precipitation technique. For the convenience of choosing the appropriate method, the advantages and disadvantages of photocatalyst preparation techniques are summarized in Table 1.

Among these methods, hydro/solvothermal seems to be very promising due to its simplicity and being an environmentally friendly process [27–31]. Recently, this method has been used to prepare  $\text{Zn}_3\text{V}_2\text{O}_7$  on graphene oxide (GO) on the nanoscale with good dispersion and high stability, which has great potential for energy storage [32]. Furthermore, the one-pot hydrothermal approach has been utilized for the synthesis of hierarchical  $\text{BiVO}_4/\text{rGO}$  with ethanolamine and polyethylene glycol as stabilizers [33]. For instance, in Fig. 3a,  $\text{N}_2$  adsorption-desorption isotherms display significantly high surface areas for  $\text{BiVO}_4/\text{rGO}$  compared to hierarchical  $\text{BiVO}_4$  and bulk  $\text{BiVO}_4$  attributed to the high specific surface area of quantum dots and rGO

**Table 1.** List of advantages and disadvantages of various photocatalyst syntheses [19–26].

Synthesis method	Advantages	Disadvantages
Hydro/solvothermal method	Controllable reaction condition followed by grain size scale, excellent dispersion, good morphology and high purity of product	Need to seal reactor, expensive autoclave, high temperature, impossibility of observing the crystal as it grows
Self-assembly procedure	Readily tuned by material composition, low cost, high throughput, simplicity, versatility	Difficulty to control in large scale
Precipitation route	High purity and excellent homogeneity of the product, short processing time, simplicity of operation	Requirement of product separation, large particles & unequal size of grains, high energy consumption, detailed communication between crystal growth & operating conditions
Sol-gel technique	Low temperature, controllable reaction during synthesis, good homogeneity, high purity and large specific surface area of product	Long process time, costly set-up materials, difficult to avoid or eliminate residual porosity, material shrinkage
Ultrasound assisted	Minimum byproduct, high selectivity, short time, high efficiency, eco-friendliness, non/low pollutions	Costly tools, requiring optimization, producing undesirable changes in molecules, process scale-up, difficulty in reactor design
Solid-state reaction method	Uniform product, good efficiency, excellent selectivity, ability to control particle size	Slowness and high energy requirement, high temperature, small surface area of the particles, and sometimes incomplete reactions

nanosheets. The photoluminescence spectra of these samples are presented in Fig. 3b. It can be seen that the intensity emission of bulk  $\text{BiVO}_4$  is more than the other ones due to the high recombination of charge carriers.

In the hydrothermal method, the solvent used in the reaction vessel is water, while in the solvothermal method an organic solvent is used to carry out the reaction [34]. For instance, Cao et al. have used a facile solvothermal process to produce  $\text{BiVO}_4$ -60 microsphere-like mesocrystals to decontaminate microcystin-LR [35]. The results of their research have shown that there is good coordination between bismuth oxide ions and acetone as a solvent. In 2022, 3D  $\text{FeVO}_4$ /nickel foam nanosheets were prepared via the hydrothermal procedure to promote the oxygen evolution reaction (OER). Iron and vanadium ions improve the electron distribution on the surface of the photocatalyst, which leads to an increase in its activity. Tan et al. have used  $\text{NH}_4\text{VO}_3$  and  $\text{Fe}(\text{NO}_3)_3 \cdot 9\text{H}_2\text{O}$  as raw materials for bamboo-like  $\text{FeVO}_4$  nanocrystalline synthesis by a two-step method of hydrothermal and calcination [36]. The energy gap of bamboo-like nanocrystals is around 2.42 eV, which is formed by the self-assembly of crystalline phases. The laboratory reactor used is called an autoclave, which must be well sealed [37]. The reactor effluent can be washed several times after filtration, which has been employed by Li et al. after the synthesis of

reduced graphene oxide (rGO)/ $\text{BiVO}_4$ /g- $\text{C}_3\text{N}_4$  [38]. In addition, Lin et al. have successfully prepared eight crystalline phases of bismuth vanadate with a controllable hydrothermal technique [39]. By controlling the temperature and acidity of the reaction environment, the desired crystal structure and morphology can be achieved [40]. In this regard, Sajid et al. [41] have prepared  $\text{FeVO}_4$  nanoparticles in a pressure container and kept at a relatively elevated temperature of up to 180 °C. The specific surface area and the mean pore diameter of  $\text{FeVO}_4$  nanoparticles have been  $89 \text{ m}^2 \cdot \text{g}^{-1}$  and 3.4 nm, respectively. The average grain size of as-synthesized powder has been 100 nm (Fig. 4).

The hydro/solvothermal method can be integrated with the calcination procedure, which has been investigated by Zheng et al. in the preparation of heterogeneous  $\text{BiVO}_4$  [42]. In addition, the surfactant-assisted hydrothermal method has been utilized to tune of developed nanorod-shape  $\text{K}_2\text{V}_3\text{O}_8$  with excellent photocatalytic activity [43]. In another research hollow microspheres of  $\text{BiVO}_4$  monoclinic have been hydrothermally synthesized in the presence of surfactant ( $\text{C}_6\text{H}_5\text{S}=\text{S}=\text{O}-\text{ONa}$ ) to introduce enriched oxygen vacancies into the bismuth vanadate [44]. Recently, it has been found that the bandgap of transition metals vanadate is in the order of  $\text{ZnV}_2\text{O}_4 > \text{BiVO}_4 > \text{FeVO}_4$  synthesized by a hydrothermal method under

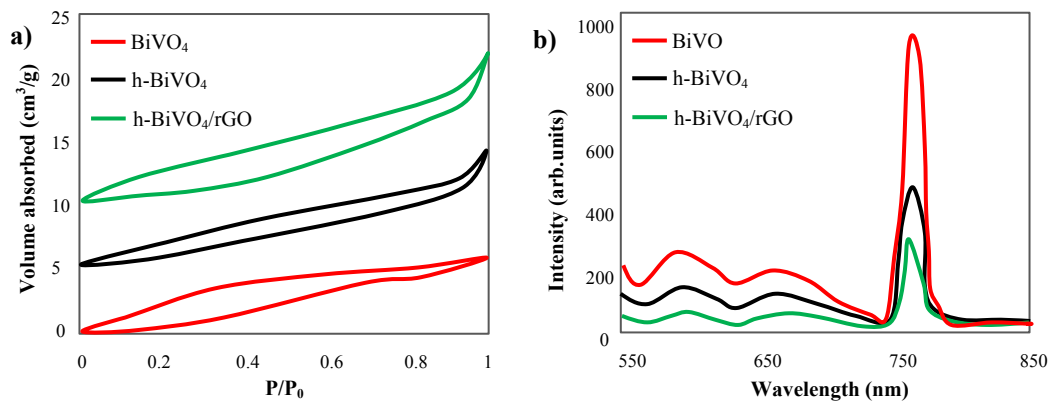


**Fig. 3.** a) Nitrogen adsorption-desorption isotherms for  $\text{BiVO}_4$ , hierarchical  $\text{BiVO}_4$  (h- $\text{BiVO}_4$ ), and h- $\text{BiVO}_4$ /rGO and b) PL spectra of  $\text{BiVO}_4$ , h- $\text{BiVO}_4$ , and h- $\text{BiVO}_4$ /rGO at RT.

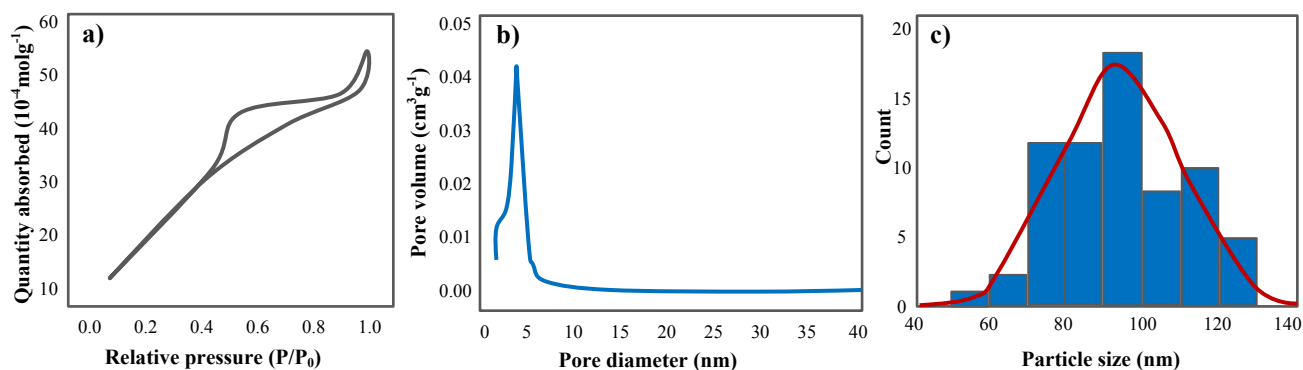


**Fig. 4.** a) Nitrogen adsorption-desorption curve for FeVO<sub>4</sub>, b) derivative pore size dispersion using Barret-Joyner-Halender (BJH) method, c) histogram of size distribution showing normal distribution behavior statistically.

200 °C and the specific surface area of ZnV<sub>2</sub>O<sub>4</sub> is higher than other compounds [45].

Self-assembly of nanomaterials is another practical way to prepare regular crystals without the intervention of external agents. It has been successfully used to construct g-C<sub>3</sub>N<sub>4</sub>/polydopamine/BiVO<sub>4</sub> nanostructure by facile ultrasonic agitation at RT [46]. The photocatalysts produced through this simple method, present high efficiency in various types of photocatalytic applications. In this method, combining individual units with a regular pattern leads to the construction of square BiVO<sub>4</sub> nanocrystals with dissolution and recrystallization, and phase transition [47]. Furthermore,

Ag<sub>3</sub>VO<sub>4</sub>/Ag<sub>4</sub>V<sub>2</sub>O<sub>7</sub> heterostructure has been synthesized during the in-situ growth of Ag<sub>4</sub>V<sub>2</sub>O<sub>7</sub> particles in a pH-adjusted one-step manner [48]. The valance band and conduction band of Ag<sub>3</sub>VO<sub>4</sub> and Ag<sub>4</sub>V<sub>2</sub>O<sub>7</sub> are shown in Fig. 5a. Almost no emission peaks are observed in the photoluminescence spectra of the Ag<sub>3</sub>VO<sub>4</sub>/Ag<sub>4</sub>V<sub>2</sub>O<sub>7</sub> nanocomposite as shown in Fig. 5b which can indicate the suppression of the recombination of charge carriers [49]. Such a Z-scheme binary photocatalyst has high efficiency and stability because of its electronic structure that allows optimum absorption of light irradiations and efficient usage of charge carriers. Lately, a simple electrostatic self-assembly method has been utilized to prepare Fe<sub>3</sub>N/BiVO<sub>4</sub> with urea as

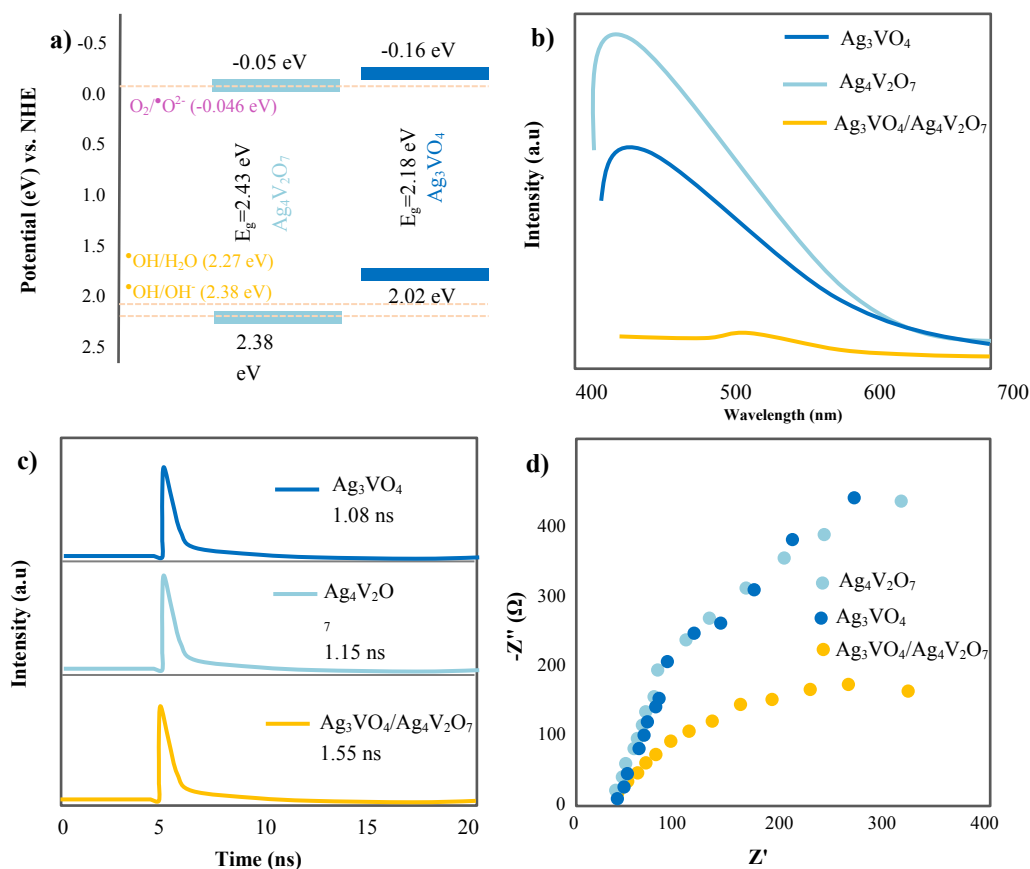


**Fig. 5.** a) Electronic structures of Ag<sub>3</sub>VO<sub>4</sub> and Ag<sub>4</sub>V<sub>2</sub>O<sub>7</sub>, b) PL spectra, c) fluorescence emission decay curves, and d) EIS Nyquist plots for Ag<sub>3</sub>VO<sub>4</sub>, Ag<sub>4</sub>V<sub>2</sub>O<sub>7</sub>, and Ag<sub>3</sub>VO<sub>4</sub>/Ag<sub>4</sub>V<sub>2</sub>O<sub>7</sub> photocatalysts.

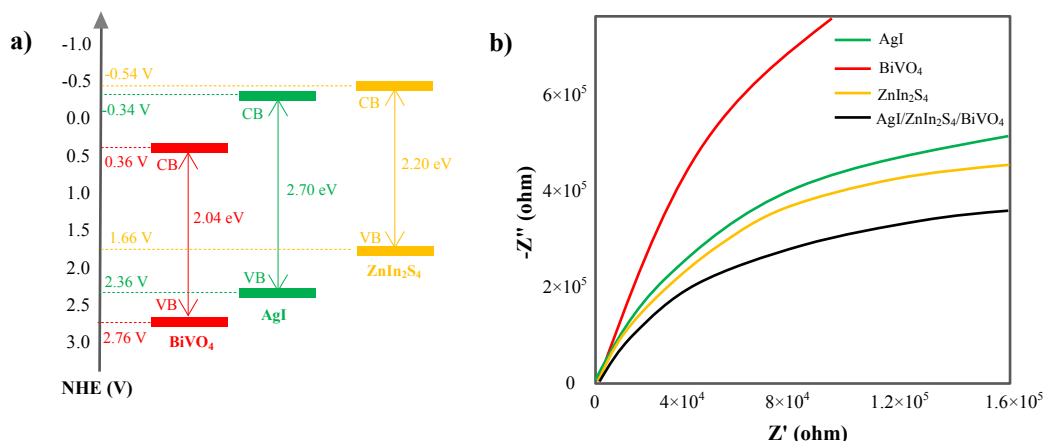


**Fig. 6.** a) The calculated bandgap of AgI, ZnIn<sub>2</sub>S<sub>4</sub> and BiVO<sub>4</sub>, b) EIS plots of AgI, ZnIn<sub>2</sub>S<sub>4</sub>, BiVO<sub>4</sub> and AgI/ZnIn<sub>2</sub>S<sub>4</sub>/BiVO<sub>4</sub>.

a nitrogen source [50]. Using this strategy, Xiao et al. have synthesized La<sub>2</sub>Ti<sub>2</sub>O<sub>7</sub>/InVO<sub>4</sub> heterojunction composites in deionized water with remarkable photocatalytic activities [51].

The precipitation technique is a common method used to synthesize vanadate nanoparticles from aqueous solutions. For this purpose, silver vanadate/bismuth-iron MOF composite nanosheets have been prepared by in situ co-precipitation approach [52]. In another study, Ghazkoob et al. tried to increase the surface area of bismuth vanadate through co-precipitation by zinc ferrite nanowires [53]. In addition, the CeVO<sub>4</sub> nanostructure has been prepared via the precipitation route by NH<sub>4</sub>VO<sub>3</sub> and Ce(NO<sub>3</sub>)<sub>3</sub>·6H<sub>2</sub>O as raw materials and hydrazine as OH<sup>-</sup> source [54]. Moreover, 3D flower-like zinc vanadate has been synthesized via this promising method with optimized process variables to modify surface morphology [55]. The monoclinic structure of BiVO<sub>4</sub> can be achieved by the co-precipitation method at a suitable calcination temperature [56]. The co-precipitation method can be carried out at room temperature, and subsequently annealing process can be used on the resulting powder, as designed by Guo et al. for the synthesis of Bi<sub>0.5</sub>Y<sub>0.5</sub>VO<sub>4</sub> solid solution [57]. In another research, Wang et al. have prepared AgI/ZnIn<sub>2</sub>S<sub>4</sub>/BiVO<sub>4</sub> composite via hydrothermal and precipitation procedure [58]. The positions of the VB and CB of these compounds are presented in Fig. 6 as a function of NHE. As shown in Fig. 6b, the EIS Nyquist plot exhibited the fastest photogenerated charge transfer performance for as-synthesized AgI/ZnIn<sub>2</sub>S<sub>4</sub>/BiVO<sub>4</sub>.

The sol-gel technique is a wet chemical method for the synthesis of

nanomaterials, turning the salts or alkoxides precursors into a gel by hydrolysis and condensation reactions. Nanoparticles of vanadate compounds can be easily prepared by this method. For example, erbium vanadate (ErVO<sub>4</sub>) nanoparticles have been prepared by the Pechini sol-gel procedure to modify the size, crystallinity, and physicochemical characteristics [59]. In another study, CuV<sub>2</sub>O<sub>6</sub>, Cu<sub>2</sub>V<sub>2</sub>O<sub>7</sub>, and Cu<sub>5</sub>V<sub>2</sub>O<sub>10</sub> crystals have been successfully prepared by adjusting the molar ratio of copper to vanadium [60]. In 2022, the sol-gel spin coating route has been used to produce homogenous V<sub>2</sub>O<sub>5</sub> and vanadium pentoxide-doped NiO in a porous structure [61]. Also, it has been observed that Bi<sub>4</sub>V<sub>2</sub>O<sub>11</sub> nanoparticles prepared by the sol-gel process are stabilized in the tetragonal phase with an average grain size of 50 nm [62].

In the sonochemical method, the ultrasonic wave causes the formation of small bubbles that grow over time and burst at high temperatures and pressures. Under these conditions, materials are produced on a smaller scale and suitable crystallinity with a higher surface area, resulting in better morphology and catalytic activity [63]. For example, BiVO<sub>4</sub>/Mg(OH)<sub>2</sub>/MoS<sub>2</sub> nanocomposites have been generated using sonicated precursors with higher e<sup>-</sup>/h<sup>+</sup> pairs separation rates than single and binary composites [64]. Recently, the rGO-ZnO-HoVO<sub>4</sub> heterostructure composites have been prepared by the ultrasonication process in an adjusted-pH solution [65]. The obtained coupled nanoparticles can be employed in the degradation of RhB. Additionally, Alijani et al. have mentioned the advantages of ultrasonic

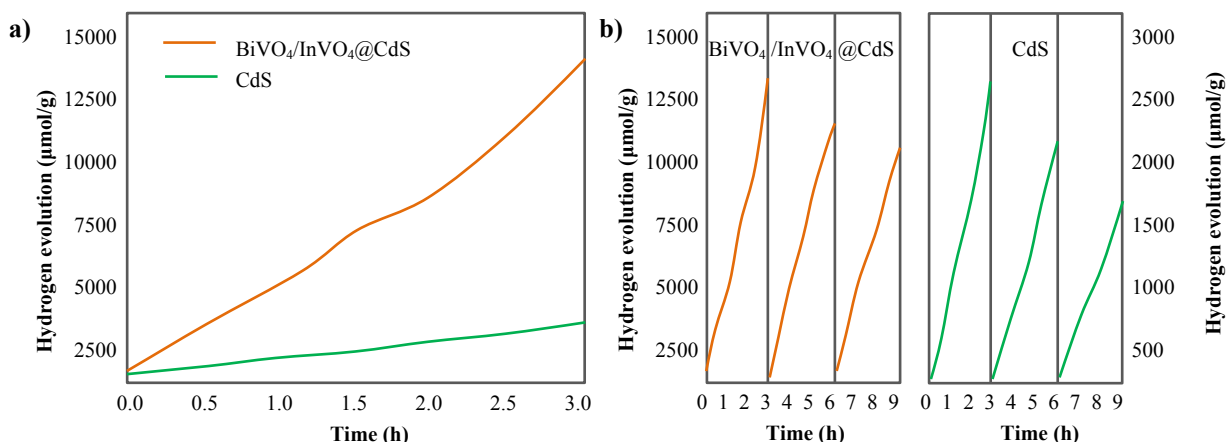


**Fig. 7.** a) Hydrogen evolution rate by BiVO<sub>4</sub>/CdS/InVO<sub>4</sub> photocatalyst compared to CdS, b) cycling test.

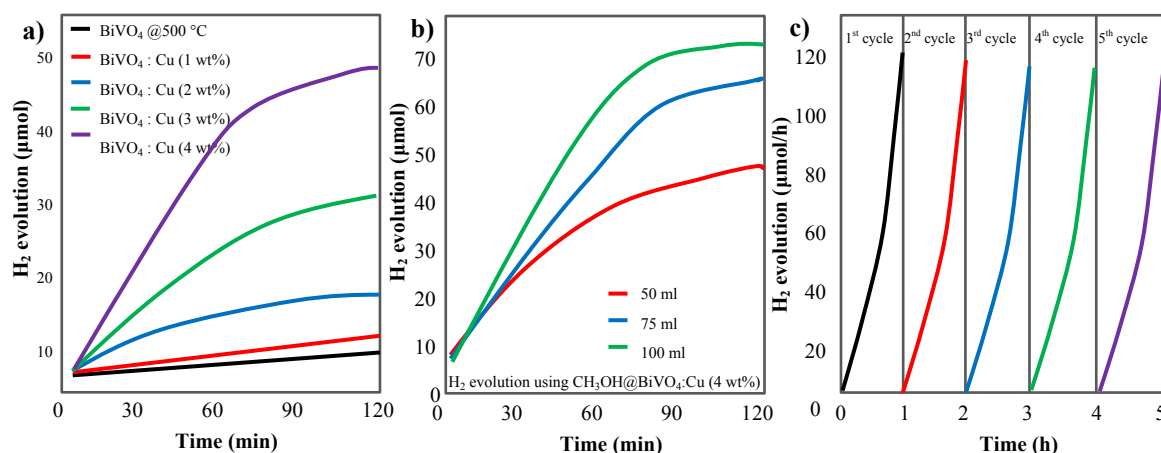


Fig. 8. a) H<sub>2</sub> evolution by Cu-doped BiVO<sub>4</sub> composites b) effect of methanol solution concentration, and c) recycling test.

and microwave-assisted synthesis methods such as simplicity, rapidness, and low energy consumption [66].

Some other research has been based on the synthesis of vanadate following solid-state reactions. In this regard, Ansari & Mohanta have designed and fabricated europium (Eu<sup>3+</sup>) doped GdVO<sub>4</sub> (gadolinium orthovanadate) photocatalyst for Congo-red photodegradation [67]. Transmission electron microscopy (TEM) imaging has shown polycrystalline nanocluster structures that are polyhedral. The solid-state method can be utilized for Ni<sub>x</sub>V<sub>2</sub>O<sub>5+x</sub> (x = 1, 2, 3) preparation as a single-component nanophotocatalyst with a small bandgap and strong ability for redox reactions [68]. The bandgap and band edge positions of nickel vanadate change by adjusting the Ni/V ratio. Furthermore, high-purity Mg<sub>2</sub>V<sub>2</sub>O<sub>7</sub> and Mg<sub>3</sub>V<sub>2</sub>O<sub>8</sub> polycrystals have been synthesized through solid-state reactions under an air atmosphere [69]. Magnesium vanadates show semiconductor behavior with appropriate bandgap through the UV-vis absorption spectrum. In the work of Patil et al., BiVO<sub>4</sub> nanostructures synthesized by solid-state reaction and hydro/solvothermal methods have been compared to construct modified structures [70]. Further, other techniques such as the soft template approach [71, 72], polymerization [73], liquid-phase exfoliation by ion exchange [74], reverses microemulsion [75], and reactive magnetron sputtering [76] have been studied in order to design and fabricate vanadate photocatalysts.

#### 4. Photocatalytic applications of vanadate compounds

Much literature has mentioned a wide variety of applications for vanadate compounds. This group of composites has important application fields such as hydrogen production, wastewater treatment, decomposition of organic contaminants in industrial effluents, and carbon dioxide reduction. In the following sections, the latest research is discussed.

##### 4.1. H<sub>2</sub> production

In the wake of global warming and the energy crisis, many researchers are trying to replace fossil fuels with solar energy to develop a sustainable society. In this regard, photocatalysis can pave the way for hydrogen production as a carbon-free green fuel during the hydrogen evolution reaction from water-splitting [77]. Various semiconductors have been investigated for this purpose, including vanadate-based compounds. Among these materials, BiVO<sub>4</sub> is a suitable semiconductor for H<sub>2</sub> generation, but it is far from industrialization. Although the main

advantages of this inorganic material, such as narrow bandgap, good visible light response, and nontoxicity make it popular. On the other hand, the photocatalytic application of bismuth vanadate is more or less limited because the produced e<sup>-</sup>/h<sup>+</sup> pairs are quickly recombined [78]. One of the primary modification methods to overcome these problems is the construction of heterojunctions. For example, BiVO<sub>4</sub> properties improve when combined with rGO nanocomposite, resulting in better H<sub>2</sub> evolution under sunlight irradiation compared to pure BiVO<sub>4</sub>. The improved performance is due to the increased surface area, better light absorption, and charge separation across the semiconductor-rGO interface generating more photoexcited charge carriers [33]. In another research, Zn<sub>m</sub>In<sub>2</sub>S<sub>3+m</sub>/BiVO<sub>4</sub> heterojunctions have been constructed for hydrogen production through visible light irradiation. Altering the Zn<sup>2+</sup>/S<sup>2-</sup> atomic ratio causes modification of the internal electric field for charge carrier separation. Density functional theory (DFT) results have shown sulfur electron transfer to oxygen for the Z-scheme construction. Zn<sub>2</sub>In<sub>2</sub>S<sub>5</sub>/BiVO<sub>4</sub> offered higher charge separation and photocatalytic activity than the other zinc-indium-sulfur species. This binary composite provides a more effective design for heterojunction solar energy conversion [79]. Shang et al. have recently investigated 2D-1D BiVO<sub>4</sub>/CdS heterostructure photocatalyst for H<sub>2</sub> energy storage and value-added chemicals production [80]. The amount of hydrogen produced during the conversion of benzyl alcohol using this combined semiconductor is 40 times higher compared to the pure BiVO<sub>4</sub> over 2 h. In another work, Fan et al. decorated BiVO<sub>4</sub>/CdS with InVO<sub>4</sub> to produce hydrogen [81]. The H<sub>2</sub> production rate by CdS and BiVO<sub>4</sub>/CdS/InVO<sub>4</sub> and the cycle test are presented in Fig. 7. The superior photocatalytic effectiveness and durability of BiVO<sub>4</sub>/CdS/InVO<sub>4</sub> are due to its impressive appearance resembling a leaf and its heterogeneous composition following a Z-scheme. In order to form a hetero-structure BiVO<sub>4</sub>-based, Imran et al. introduced ZnCdS to positively affect the properties of nanocomposite in a double pathway i.e., reduction of photocorrosion and enhancement of the sunlight absorption [82]. The encapsulation of BiVO<sub>4</sub> with transition metals such as copper has been suggested by Manikantan et al. to extend the sensitivity of BiVO<sub>4</sub> to the visible spectrum allowing H<sub>2</sub> production under sunlight irradiation [83]. The effect of the weight percentage of Cu as a dopant, the amount of methanol consumed as a sacrificial factor, and recyclability in the hydrogen production stability test are shown in Fig. 8. The Cu 4 wt%:BiVO<sub>4</sub> exhibits steady activity after 2 h under irradiation. After the fourth cycle, it decreases slightly



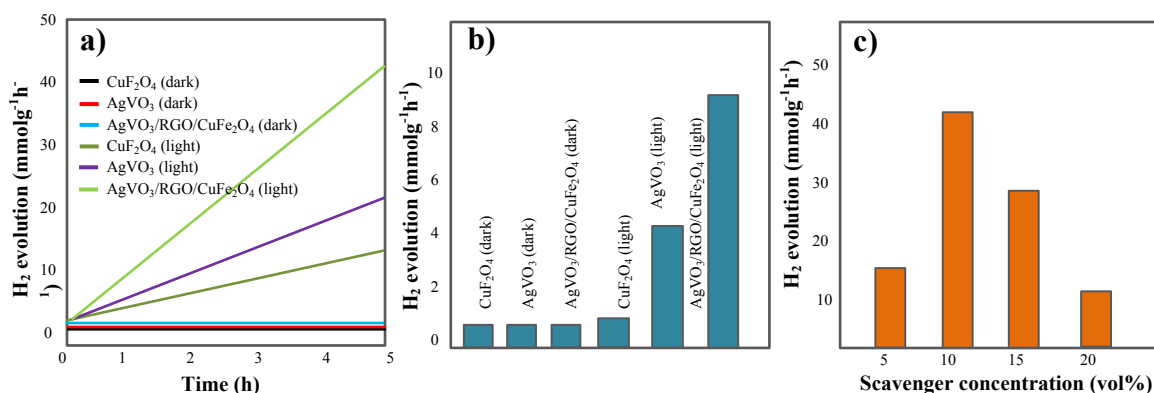


Fig. 9. a) H<sub>2</sub> production vs time, b) average H<sub>2</sub> evolution rate, and c) effect of the lactic acid on H<sub>2</sub> evolution.

because of sacrificial agent consumption. Pure InVO<sub>4</sub> is rarely utilized for water photosplitting due to the short distribution length of  $h^+$ . To deal with this problem, surface polarization can be used to increase the efficiency of H<sub>2</sub> and O<sub>2</sub> production from water [84]. Hydroxyl groups modify inorganic acids to ionize in the solution and cause more negative charges carried by InVO<sub>4</sub>. The diffusion length of photogenerated holes increases by electromagnetic field induction and flows to the surface.

Innovations in photocatalytic water-splitting can be facilitated through the manufacture of photocatalysts composed of MXenes [85]. It has been reported that ultrathin MXene/BiVO<sub>4</sub> nanosheets display high photoexcited  $e^-/h^+$  transfer and separation efficiency in H<sub>2</sub> production [86]. Also, the photocatalytic activity of CdS/BiVO<sub>4</sub>/MXene synthesized by two steps has been compared with pure CdS and BiVO<sub>4</sub> in H<sub>2</sub> generation performance by Wang et al. [87]. They indicated that charge transfer and separation of photoinduced  $e^-/h^+$  increase by loading MXene as a cocatalyst. In another study, Ti<sub>3</sub>C<sub>2</sub> MXene quantum dots effect has been investigated on as-prepared ZnIn<sub>2</sub>S<sub>4</sub>/BiVO<sub>4</sub> via a two-step solvothermal method [88]. Quantum dots of Ti<sub>3</sub>C<sub>2</sub> can increase the hydrogen generation rate up to 103  $\mu\text{mol.g}^{-1}.\text{h}^{-1}$  beside ZnIn<sub>2</sub>S<sub>4</sub>/BiVO<sub>4</sub>.

Carbon nitride (CN) is another popular compound in synthesizing binary and ternary photocatalysts that are used in hydrogen evolution reactions. The main obstacle to the low performance of pure CN is the incorporation of charge carriers, which has decreased with the advent of heterojunction technology, hoping to fabricate suitable photocatalyst composites. In an innovative heterojunction design, BiVO<sub>4</sub>/modified CN has been prepared for H<sub>2</sub> generation from water-splitting by Hayat et al. [89]. They have shown that BiVO<sub>4</sub>/CN as a superior catalyst exhibits high efficiency in hydrogen production when exposed to the visible light spectrum. In another research, CN has been tested in the construction of rGO/InVO<sub>4</sub>/g-C<sub>3</sub>N<sub>4</sub> ternary nanocomposite using a wet impregnation technique [90]. By consolidation of InVO<sub>4</sub> and rGO into g-C<sub>3</sub>N<sub>4</sub>, the photocatalysts absorption edge of CN has been significantly boosted from 451 nm (2.75 eV) to 546 nm (2.27 eV), thanks to the created heterojunction. Notably, g-C<sub>3</sub>N<sub>4</sub> loaded with varying weight percentages of InVO<sub>4</sub> and rGO displayed different outcomes. Specifically, g-C<sub>3</sub>N<sub>4</sub> with a loading of 3.0 wt% of rGO and 30 wt% of InVO<sub>4</sub> has exhibited exceptional hydrogen production of 7449  $\mu\text{mol.g}^{-1}.\text{h}^{-1}$ . This represents a remarkable improvement of 45 times compared to a single g-C<sub>3</sub>N<sub>4</sub>. Photoluminescence and photocurrent studies have demonstrated that the InVO<sub>4</sub>/g-C<sub>3</sub>N<sub>4</sub>

heterojunction, in conjunction with the rGO support, effectively enhances the separation and transportation of charge carriers. In addition, the rate of hydrogen production observed in the current binary nanocomposite was nearly 35-fold greater than the hydrogen production rate documented in Hu et al. research on binary InVO<sub>4</sub>/g-C<sub>3</sub>N<sub>4</sub> nanocomposites that lacked rGO support [91]. In another work, the amount of hydrogen production using InVO<sub>4</sub>/g-C<sub>3</sub>N<sub>4</sub> with carbon quantum dots (CQDs) hardly reaches 2170  $\mu\text{mol.g}^{-1}.\text{h}^{-1}$  [92] indicating the superiority of rGO over CQDs in photocatalytic H<sub>2</sub> evolution. In 2022, InVO<sub>4</sub>-based heterojunctions of BiVO<sub>4</sub> with CdS as electron mediators were fabricated regarding H<sub>2</sub> generation [93]. Leaf-like structure InVO<sub>4</sub>/BiVO<sub>4</sub>/CdS has elevated the H<sub>2</sub> production rate to 5.03  $\text{mmol.g}^{-1}.\text{h}^{-1}$ . Moreover, it has been reported that polymeric-C<sub>3</sub>N<sub>4</sub> with InVO<sub>4</sub> is an effective photocatalyst for solar-to-hydrogen conversion with a maximum activity of  $\sim 9 \text{ mmol.g}^{-1}.\text{h}^{-1}$  [94].

In 2022, Alkorbi et al. reported the usage of SmVO<sub>4</sub> nanoparticles with sulfur self-doped C<sub>3</sub>N<sub>4</sub> (SCN) to form of type II heterostructure [95]. Decorated SmVO<sub>4</sub> has a lower bandgap (1.89 eV) compared to SCN (2.44 eV) and pure SmVO<sub>4</sub> (2.16 eV). Therefore, SmVO<sub>4</sub>/SCN has a high hydrogen evolution potential of 22.618  $\text{mmol.g}^{-1}$  during 4 h under photochemical conditions. Such a nanocomposite photocatalyst can generate sufficient H<sub>2</sub> for energy storage. In another work, Sun et al. switched the photoexcited  $e^-/h^+$  pairs transfer pathway of polymeric carbon nitride (PCN)/BiVO<sub>4</sub> heterojunction photocatalyst from type-II to Z-scheme [96]. The direct Z-scheme photocatalysts, specifically PCN and BiVO<sub>4</sub> enhance water photosplitting without acidity adjustment or any sacrificial agents. Furthermore, PCN has been hybridized with CoV<sub>2</sub>O<sub>6</sub>.2H<sub>2</sub>O by the immersion approach to promote the performance of the water-splitting reaction under UV and visible light irradiation [97]. The narrow bandgap of CoV<sub>2</sub>O<sub>6</sub> (2.03 eV) harvests sunlight and enhances CoV<sub>2</sub>O<sub>6</sub>/PCN light sensitivity which is favored for the H<sub>2</sub> and O<sub>2</sub> production. A 2D/2D g-C<sub>3</sub>N<sub>4</sub>/LaVO<sub>4</sub> heterostructure could be an efficient photocatalyst for producing H<sub>2</sub> and furfural simultaneously [98]. The well-formed hetero-interfaces of g-C<sub>3</sub>N<sub>4</sub> and LaVO<sub>4</sub>, using furfuryl alcohol as a hole sacrificial agent substitute triethanolamine, enable to increase in H<sub>2</sub> evolution rate three times more than pure g-C<sub>3</sub>N<sub>4</sub>. Moreover, the S-scheme heterojunction of BiVO<sub>4</sub> and Bi<sub>0.6</sub>Y<sub>0.4</sub>VO<sub>4</sub> leads to a significant enhancement of water-splitting efficiency compared to bare BiVO<sub>4</sub> [99]. Carrier dynamics has determined that photoinduced charge separation through S-scheme heterojunctions significantly affects the progress of the hydrogen production reaction.

It has been also found that silver vanadate ( $\text{AgVO}_3$ ) is more promising in absorbing visible light, while iron vanadate ( $\text{FeVO}_4$ ) competes in photoelectrochemical conversion. [100]. Although the performance of  $\text{AgVO}_3$  is limited due to the ease of recombination of charge carriers, this defect can be overcome with new strategies. Hence, the heterostructure of  $\text{AgVO}_3/\text{Ag}/\text{SnS}_2$  has been fabricated via the hydrothermal method [101]. The  $\text{AgVO}_3/\text{Ag}/\text{SnS}_2$  composite has exhibited a  $2.8 \text{ mmol.g}^{-1}\text{h}^{-1}$   $\text{H}_2$  production rate under the sunlight spectrum. This photocatalyst maintains its stability after 8 consecutive cycles, and its efficiency decreases slightly. Another effective sulfur compound to pair with silver vanadate is CdS, which accelerates the separation of charge carriers [102]. By constructing a p-n type of  $\text{AgVO}_3/\text{CdS}$  composite through loading  $\text{AgVO}_3$  on CdS hexagonal nanorods, the visible light absorption is improved. In another study,  $\text{AgVO}_3/\text{Fe}_2\text{O}_3$  mesopores were fabricated by the wet-impregnation method for energy production [103]. The core-shell structure of  $\text{AgVO}_3/\text{Fe}_2\text{O}_3$  has caused the enhancement of the photocatalyst surface and light absorption ability and facilitates charge separation. In another study, irregularly shaped  $\text{CuFe}_2\text{O}_4$  and rod-like  $\text{AgVO}_3$  were distributed on rGO nanosheets [104]. This novel composite achieved  $9 \text{ mmol.g}^{-1}\text{h}^{-1}$  hydrogen evolutions with high stability and recyclability (Fig. 9). As shown in Fig. 9c, the volume consumption of the scavenger agent (lactic acid) rapidly affects the rate of hydrogen production. The heterogeneity of  $\text{CuFe}_2\text{O}_4/\text{AgVO}_3/\text{rGO}$  makes it a superior semiconductor capable of rapidly separating charge carriers for photocatalytic  $\text{H}_2$  generation.

#### 4.2. Removal of pollutants

Currently, many scientists are focused on industrial wastewater treatment by real and synthetic photocatalysts. As mentioned above, a semiconducting system's catalytic efficiency is affected by various factors, including light energy harvest, specific surface area,  $e^-/h^+$  pair's generation, interface bonding, and photoinduced charge transport ability. Vanadate-based heterojunction forms many materials with these features [105]. In addition, the manufacture of a photocatalytic system that utilizes solid-state carrier transport to prompt a Z-scheme has a significant potential for eco-friendly technology as it allows for effective separation and transfer of carriers in a hybrid heterojunction, which offers a novel method to enhance the performance of sunlight-driven photocatalysis as opposed to traditional composites [106]. Photocatalysts based on  $\text{BiVO}_4$  are the most well-known and popular materials for removing various drugs from water. For example, the  $\text{Ag}_2\text{MoO}_4/\text{BiVO}_4$  composite shows complete removal of 17 $\alpha$ -ethinyl estradiol in 40 min under visible light irradiation [107]. In addition,  $\text{InVO}_4$  hybridized photocatalysts emphasize the degradation of drugs, especially antibiotics [108]. In one case,  $\text{InVO}_4/\text{Ag}/\text{g-C}_3\text{N}_4$  has been designed and tested for removing amoxicillin in wastewater treatment. Silver improved electron transfer between  $\text{InVO}_4$  and  $\text{g-C}_3\text{N}_4$ , effectively absorbing visible light and producing electrons in the  $\text{g-C}_3\text{N}_4$  conduction band and holes in the  $\text{InVO}_4$  valence band. Electrons react with  $\text{O}_2$  to form radicals, degrading amoxicillin, and holes oxidize antibiotics to degradation. The synthesized  $\text{InVO}_4/\text{Ag}/\text{g-C}_3\text{N}_4$  has shown advanced photocatalysis for amoxicillin removal, with high

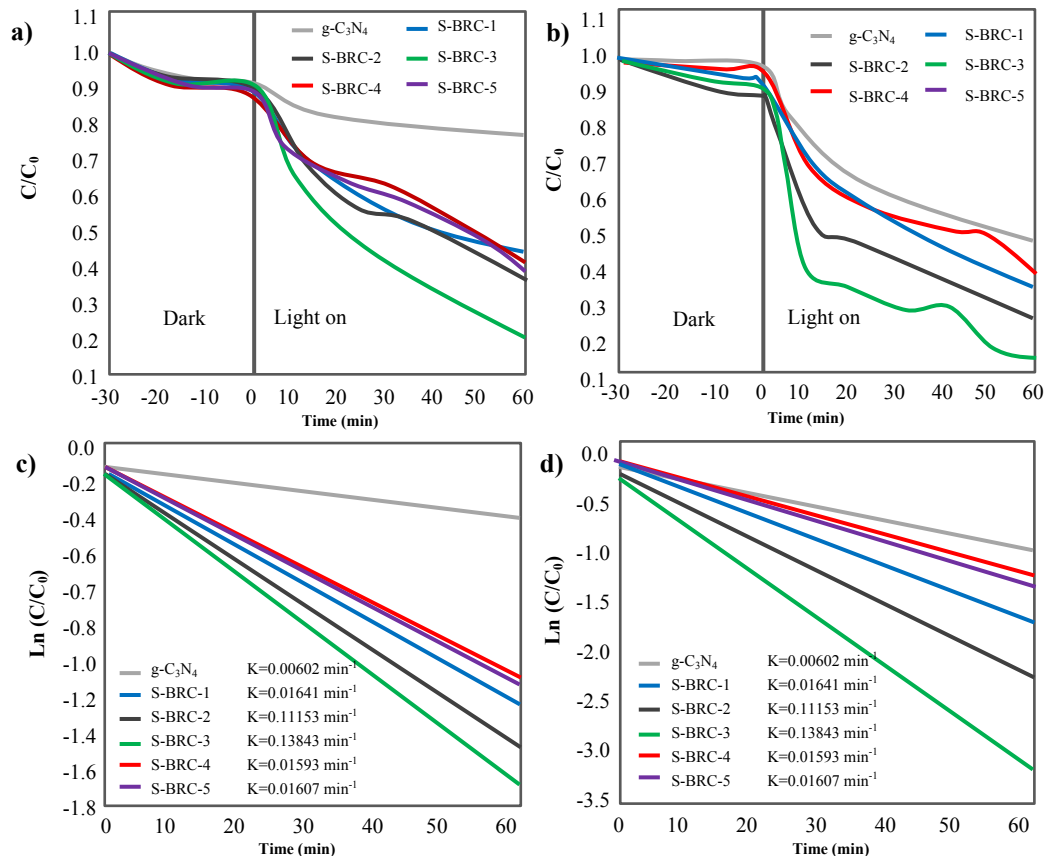


**Fig. 10.** a, b) Photocatalytic degradation activity of tetracycline and ciprofloxacin and c, d) kinetic plots of degradation by  $\text{BiVO}_4/\text{rGO}/\text{g-C}_3\text{N}_4$  and pure  $\text{g-C}_3\text{N}_4$  composites.



stability and recycling ability [109]. Another vanadate-based semiconductor is  $\text{Ag}_3\text{VO}_4$  which has great potential for tackling the antibiotics in waterways [110].

One of the main photocatalytic research interests is creating a Z-scheme complex for photocatalysis that possesses optimal energy band positioning and redox capacity. In that direction, Li et al. have employed a singular hydrothermal technique to merge Z-scheme  $\text{BiVO}_4/\text{rGO}/\text{g-C}_3\text{N}_4$  nanocomposites with spindle-like shapes, using sodium oleate as a surfactant [38]. Utilizing the ultrathin  $\text{g-C}_3\text{N}_4$  nanosheets and spindle-shaped  $\text{BiVO}_4$ , the composite photocatalysts provide a significant surface for light absorption and reactions. The photodegradation of antibiotics through photocatalysis results in a significant reduction in tetracycline and ciprofloxacin, with degradation rates up to 81% and 95% within an hour, respectively (Fig. 10). The ternary composite exhibit better photocatalytic efficiency compared to other its pure compounds either  $\text{rGO}/\text{g-C}_3\text{N}_4$  [111]. The exceptional optical capabilities, directed carrier transportation, and photooxidation response of spindle-shaped  $\text{BiVO}_4$  nanostructures overcome the limited carrier's diffusion length in typical  $\text{BiVO}_4$  photocatalysts, which results in an apparent recombination rate for electron-hole pairs. Also, for the ciprofloxacin photooxidation,  $\text{AgVO}_3$ -anchored 2D  $\text{CeO}_2$  nanocrystals have been designed and constructed through a precipitation method [112]. The  $\text{CeO}_2/\text{AgVO}_3$  p-n heterojunction has shown 96% of recyclability after the 5th consecutive cycle. Furthermore,  $\text{rGO}$  has been used to design and fabricate  $\text{rGO-Mn}_2\text{V}_2\text{O}_7$  composites via a simple one-pot hydrothermal hybridization in order to ciprofloxacin degradation. This economical and reusable photocatalyst demonstrates a high performance of catalytic materials after several rounds of usage

[113]. Other binary photocatalysts that have been tested with  $\text{rGO}$  are  $\text{g-C}_3\text{N}_4/\text{BiVO}_4$ , which use  $\text{g-C}_3\text{N}_4$  layered sheets and distinct  $\text{BiVO}_4$  quantum dots to improve photoabsorption and surface promotion [114]. The preparation of quantum dots on bismuth vanadate is the responsibility of the surfactant  $\text{C}_{18}\text{H}_{33}\text{NaO}_2$  (sodium oleate), and in this way, the Z-scheme photocatalyst with high ability in redox reactions for the destruction of antibiotics is assembled. The Montmorillonite-supported  $\text{BiVO}_4$  composite has recently been suggested to remove Brilliant Red 80 dye from wastewater under visible light range by Akhter et al. [115]. The photocatalytic degradation activity of Montmorillonite/ $\text{BiVO}_4$  is about 100% at 2 h after irradiation, while pure  $\text{BiVO}_4$  shows ~80% decomposition.

Solar-based Z-scheme photocatalysts have the potential to solve energy shortages and environmental problems [116]. Hence, a dual Z-scheme heterojunction of  $\text{SmVO}_4/\text{Co}_3\text{O}_4/\text{CuBi}_2\text{O}_4$  has been employed for carbamazepine degradation under the Xe lamp [117]. The degradation efficiency of this anticonvulsant drug is boosted with oxidants and achieves 76% of removal in the presence of the  $\text{SmVO}_4/\text{Co}_3\text{O}_4/\text{CuBi}_2\text{O}_4$  ternary composite after 5 h (Fig. 11). Furthermore,  $\text{SmVO}_4$  decorated  $\text{g-C}_3\text{N}_4$  is a visible light active photocatalyst for removing hazardous chloramphenicol drugs and amaranth dye with 94 and 99% efficiency, respectively [118].  $\text{SmVO}_4$  has been tested with sulfur-doped  $\text{g-C}_3\text{N}_4$  in the degradation of methyl orange (MO). The high yield (90%) in a short period of time (80 min) has been attributed to the formation of a type II heterostructure [95]. On the other hand, rod-like  $\text{SmVO}_4$  is used alone to degrade tetracycline and maintains its efficiency in three consecutive cycles [119]. Another vanadate compound for the degradation of tetracycline

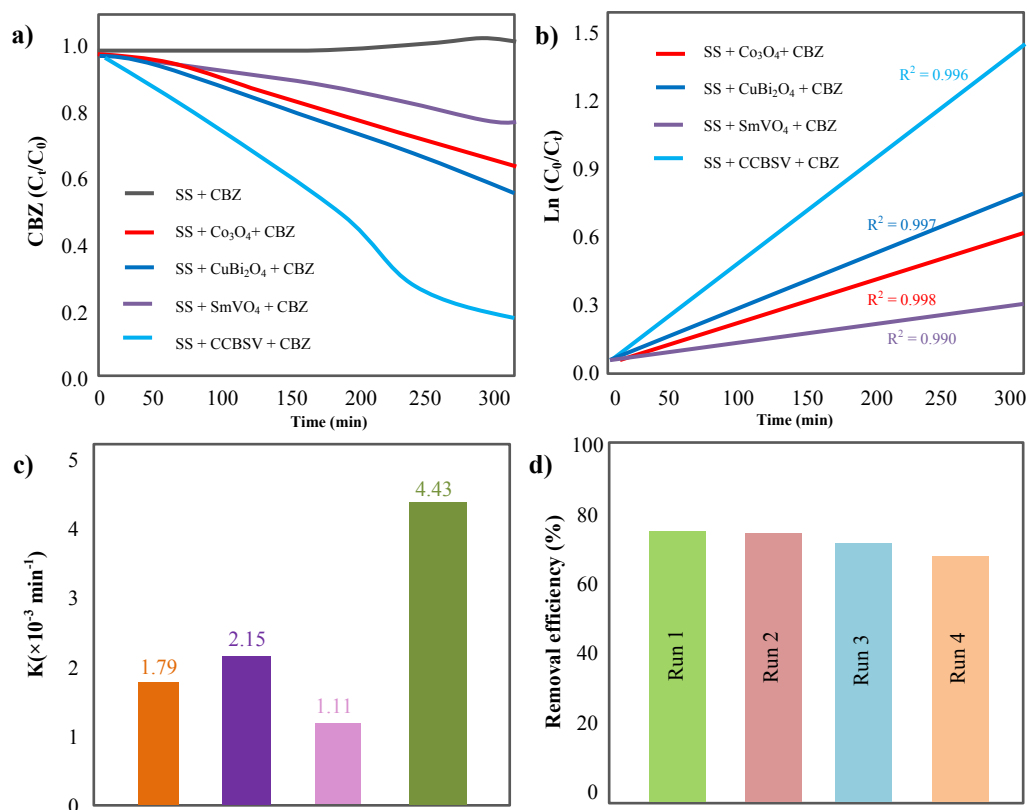


**Fig. 11.** a) Influence of illumination time on the photodegradation of carbamazepine, b) Pseudo-first-order plots of  $\text{Co}_3\text{O}_4$ ,  $\text{CuBi}_2\text{O}_4$ ,  $\text{SmVO}_4$ , and  $\text{Co}_3\text{O}_4/\text{CuBi}_2\text{O}_4/\text{SmVO}_4$ , c) rate constant of degradation reaction by  $\text{Co}_3\text{O}_4$ ,  $\text{CuBi}_2\text{O}_4$ ,  $\text{SmVO}_4$ , and  $\text{Co}_3\text{O}_4/\text{CuBi}_2\text{O}_4/\text{SmVO}_4$ , d) degradation efficiency after several runs.

is  $\text{AgVO}_3$  incorporated  $\text{Bi}_4\text{Ti}_3\text{O}_{12}$  in the form of a Z-scheme heterojunction [120]. The  $\text{Bi}_4\text{Ti}_3\text{O}_{12}/\text{AgVO}_3$  composite has exhibited 57% degradation efficiency of tetracycline within 1 h. Meanwhile, activated biochar/ $\text{BiVO}_4$  heterojunction nanocomposite could altogether remove tetracycline from the surface water [121]. Additionally, biochar/ $\text{BiVO}_4$  has displayed a degradation efficiency of norfloxacin and chloramphenicol of more than 72% at 2 h.

The presence of synthetic dyes, including methylene blue (MB), Rhodamine B (RhB), and methyl orange (MO), in industrial and textile effluents is increasing due to high demand [122, 123]. For this purpose, Chen et al. have created a p-n heterojunction of halloysite nanotubes supported by  $\text{BaSnO}_3/\text{BiVO}_4$  by a facile precipitation method for methylene blue dye degradation [124]. They have shown that the composite exhibits significant catalytic efficiency, with a decolorization rate of 94% after 2 hours of visible spectrum exposure, surpassing  $\text{BaSnO}_3$ ,  $\text{BiVO}_4$  even  $\text{BaSnO}_3/\text{BiVO}_4$ . In another work,  $\text{ErVO}_4$  nanoparticles have been used as a narrow bandgap compound for the photocatalytic removal of MB dye under UV light [125].  $\text{ErVO}_4$  nanostructure showed 80% degradation efficiency in the optimum loading amount of photocatalyst. In addition, synthesized  $\text{KV}_3\text{O}_8$  and  $\text{K}_2\text{V}_6\text{O}_{16} \cdot n\text{H}_2\text{O}$  have been evaluated for MB dye photodegradation under simulated sunlight irradiation [74]. The micro platelets of  $\text{KV}_3\text{O}_8$  displayed the most noteworthy photocatalytic capability, leading to the degradation of over 90% of the dye in the first half-hour at 80 °C. The high efficiency of photocatalysis is considered due to the significant presence of  $\text{V}^{4+}$  ions. Deka et al. have recently synthesized  $\text{BiVO}_4$  nanorods with high content of oxygen defects for MB degradation [126]. In a time frame of 40 minutes, the degradation of MB dye has been observed to be 97.6% and 97.1% through photocatalytic and piezo-photocatalytic means, respectively. The piezo-photocatalysis prevails for a brief duration, and then it gradually decelerates over time due to the ruin of active sites of  $\text{BiVO}_4$  by sonication's fracturing effect. To eliminate MB dye, indium vanadate is another semiconductor that can be doped with copper [127]. The presence of oxygen vacancies, Cu dopant, and  $\text{V}^{4+}/\text{V}^{5+}$  ions in  $\text{Cu-InVO}_4$  resulted in better photon absorption and photocatalytic performance as compared to pure  $\text{InVO}_4$ . Complete removal of MB dye at pH 6 is achieved under LED light irradiation while in the research of Manikantan et al. Cu-encapsulated  $\text{BiVO}_4$  nanosheets decompose the whole MB dye under the visible spectrum [83]. Newly, vanadium pentoxide ( $\text{V}_2\text{O}_5$ ) decorated with chitosan-anisaldehyde has been investigated for MB degradation by Bansal et al. [128]. They have found that the execution of this composite was severely influenced by the  $\cdot\text{O}_2^-$  as an active species of scavenger in the degradation process, which caused a diminishing from 92% to 36%. Also,  $\text{BiVO}_4$  sheets with  $\text{g-C}_3\text{N}_4$  have been hydrothermally prepared to degrade Rhodamine B dye under direct sunlight [129]. More than 90% degradation efficiency was obtained in 2 hours, which is attributed to hydroxyl and superoxide radicals. It has been suggested a charge transfer mechanism photocatalysis improved due to recombination inhibition, efficient carrier transfer, and high reactive species production. In another research, rGO has been tested as a support  $\text{ZnO}/\text{HoVO}_4$  composites to enhance the degradation of Rhodamine B dye under UV light irradiation. This coupled photocatalyst can increase the efficiency of the process to more than 70% in 45 minutes, while each of the composites has barely reached 58% efficiency [65]. Following the efforts of Wannakan et al., the S-scheme  $\text{BiVO}_4/\text{ZnO}$  nanocomposite has been successfully constructed for the degradation of the Reactive

Red 141 Dye [130]. Complete detoxification of this harmful pollutant has been achieved under sunlight irradiation.

Malachite green (MG) dye is another contaminant that would remove from water and other effluents by vanadate photocatalyst. In one case,  $\text{Co}_3\text{V}_2\text{O}_8$  nanoparticles produced at the scale of 40 nm can achieve up to 90% removal efficiency in 60 minutes [131]. In another study, MG dye degradation by active  $\text{BiVO}_4$  nanoparticles has been investigated through various parameters (concentration, pH, and time) under solar light irradiation. Within less than 1 h, bismuth vanadate nanocomposites have demonstrated a 95% yield of the process [132]. In addition, elemental doping, such as noble metals, is an interesting way to enhance the activity of vanadate compounds. In this regard, Channei et al. fabricated Pd doped- $\text{BiVO}_4$  through a microwave-

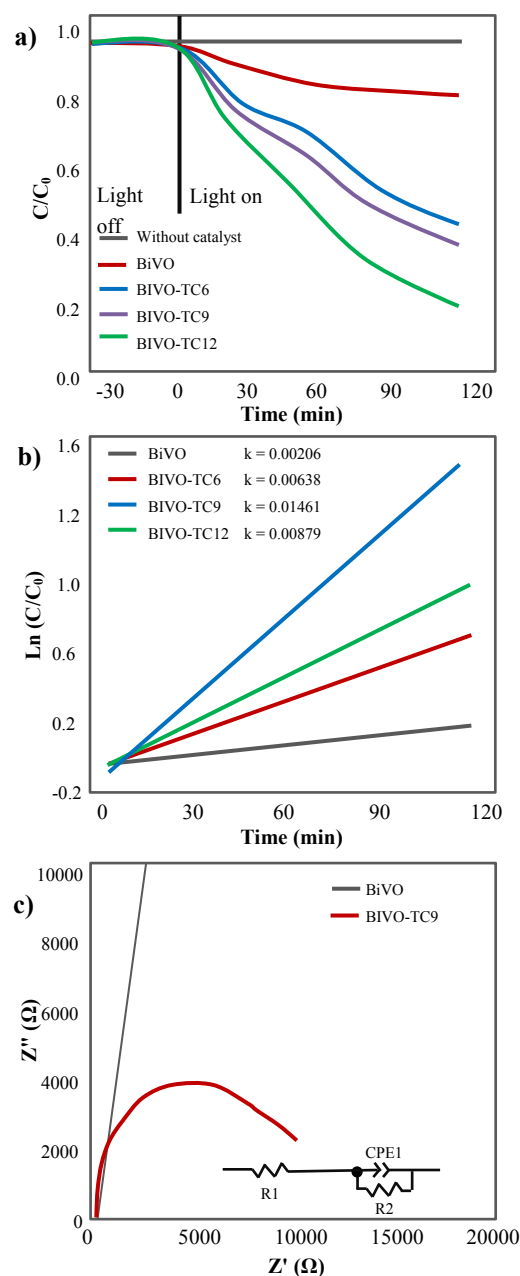


**Fig. 12.** a) photocatalytic curves of Cr reduction, b) first-order plots for the removal of Cr, and c) PL spectra.

assisted approach for MG dye degradation [133]. The photoluminescence spectrum (PL) has indicated a lower recombination of  $e^-/h^+$  pairs by the construction of Pd/BiVO<sub>4</sub>. The as-prepared sample could achieve 98% degradation efficiency under the visible spectrum, which is 5 times greater than a single BiVO<sub>4</sub> and reusable for 3 continuous cycles. In another work, the photoreduction of MG dye has been compared with surfactant-free and surfactant-assisted Cu<sub>2</sub>V<sub>2</sub>O<sub>7</sub> [134]. The surfactant sample shows higher degradation efficiency because the surfactant (polyvinyl pyrrolidone) acts as an  $e^-/h^+$  trap.

Photocatalytic degradation of pesticides under the light spectrum leads to chemical conversions. During the process, superoxide and hydroxyl species are released, which play a crucial role in the photolytic destruction of pesticides [135]. In this regard, TiO<sub>2</sub> nanotubes/BiVO<sub>4</sub>/rGO photocatalyst has been hydrothermally prepared via a one-step strategy by Piao et al. for the removal of imidacloprid insecticide [136]. They have shown that the dosage of ternary composite, pH, and loading amount of TiO<sub>2</sub>/rGO affects the degradation efficiency. Furthermore, this semiconductor can degrade up to 74% of imidacloprid within 0.5 h under the UV spectrum and reuse for six continuous cycles without apparent efficiency loss. In another study, bio-fabricated BiVO<sub>4</sub> by *Curcuma longa* through hydrolysis has been introduced as a supramolecular organic composite for decomposing an organochlorine pesticide under LED light [137]. The flower-like *Curcuma longa*-mediated bismuth vanadate has exhibited a 90% degradation efficiency of 2,4-dichlorophenoxy acetic acid during 2 h, while pure BiVO<sub>4</sub> has 46% fragmentation efficiency.

#### 4.3. Removal of heavy metals

Another application of photocatalysts based on vanadate compounds is the elimination of heavy metal ions from wastewater, which is known as an environmentally friendly method with industrial prospects. Treatment of wastewater containing chromium is necessary to deal with the threat to human, animal, and plant health. For this purpose, Wang et al. have fabricated a visible-light-driven type II photocatalyst by C<sub>3</sub>N<sub>4</sub>/BiVO<sub>4</sub> and Ag<sub>3</sub>VO<sub>4</sub> which has a Cr reduction rate of about 20-fold greater than pure BiVO<sub>4</sub> [138]. Another effective way is the deposition of BiVO<sub>4</sub> on MIL-101-NH<sub>2</sub> without surfactant with excellent reusability for the removal of Cr [139]. The stability of this composite is attributed to the ionic bond Bi<sup>3+</sup>-COO<sup>1-</sup>, which increases the affinity of MIL-101-NH<sub>2</sub> and BiVO<sub>4</sub>. Also, the reduction of Cr(VI)

is promoted by p-n heterostructure BiVO<sub>4</sub>/polyaniline photocatalyst [140]. Furthermore, the coating of CuS particles on BiVO<sub>4</sub>/Fe<sub>3</sub>O<sub>4</sub> provides a recyclable heterogeneous photocatalyst boost of Cr(VI) reduction [141]. It is reported that 2D/2D MXene/BiVO<sub>4</sub> heterojunction is an excellent photocatalyst for removing Cr(VI) by solar-light-driven process, as shown in Fig. 12 [142]. The MXene/BiVO<sub>4</sub> nanocomposite could achieve up to 84% of photocatalytic efficiency after 2 h. In addition, Luo et al. have demonstrated that a Z-scheme protonated BiVO<sub>4</sub>/wood flour biochar/g-C<sub>3</sub>N<sub>4</sub> semiconductor provides directional charge-transfer pathways and effective separation of photoinduced  $e^-/h^+$  pairs [143]. Moreover, introducing graphene oxide (GO) into BiVO<sub>4</sub> could notably increase the photocatalytic activity under the visible light spectrum for Cr removal [144]. In another research, yttrium-doped TiO<sub>2</sub>/BiVO<sub>4</sub> has been applied to reduce Cr(VI) to Cr(III) [145]. Zahoor et al. have demonstrated the effect of each compound on the photocatalyst improvement, which causes synergy in the photoreduction of chromium. In order to remove copper from water, optimized photocatalyst BiVO<sub>4</sub>/rGO/g-C<sub>3</sub>N<sub>4</sub> has achieved up to 90% reduction efficiency [146]. It has been proved that photoinduced electrons are primarily responsible for Cu reduction. Mercury (Hg<sup>2+</sup>), is another ion that is a severe environmental pollutant that slowly accumulates in water sources and enters the human food chain. Recently, Alhaddad et al. have removed mercury (II) ions almost completely by utilizing BiVO<sub>4</sub>/ZnO p-n heterojunction under visible light irradiation [147]. This photoreduction efficiency (100%) has been obtained with 3 wt% of homogeneous BiVO<sub>4</sub> nanoparticles within 45 minutes. The heterostructures of ZnO mesopores coupling with BiVO<sub>4</sub> nanoparticles are 14-fold capable of activity compared to bare ZnO.

#### 4.4. CO<sub>2</sub> reduction

Through the combustion of fossil fuels, environmental crises are increasing along with CO<sub>2</sub> emission, which has led to ecological changes and greenhouse effects [148]. Therefore, converting CO<sub>2</sub> into valuable hydrocarbon materials using sunlight absorption can be a solution to compensate for the lack of energy and solve environmental problems [149]. Among synthetic semiconductors, photocatalysts based on vanadate compounds are increasingly used for CO<sub>2</sub> reduction. It has been found that doped BiVO<sub>4</sub> can have significant photocatalytic activity for CO<sub>2</sub> conversion [150]. Co-doping of Tm/Sm ions can adjust the solid band structure, provide additional light absorption, and

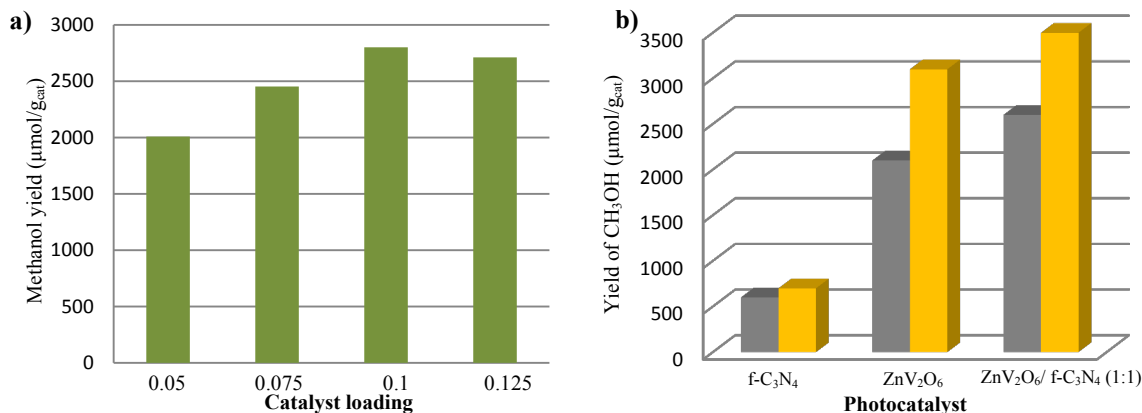


Fig. 13. a) The effect of cocatalyst amount and b) comparison between the solar reactor and externally reflected reactor.

facilitate the separation of charge carriers to produce methane and carbon monoxide. Furthermore, the deposition of noble metals on the  $\text{BiVO}_4$  causes electron migration across the Schottky junction and suppresses the passage of electrons in the opposite direction [151]. Recently indium vanadate-based photocatalysts have attracted many scientists for the photoreduction of  $\text{CO}_2$  due to the remarkable catalytic activity of  $\text{InVO}_4$ . In one case, Wei et al. [152] designed and synthesized a novel Z-scheme  $\text{InVO}_4/\text{CoAl}$  (cobalt aluminum)-LDH (layered double hydroxides) heterojunction for enhancing photocatalytic  $\text{CO}_2$  reduction.  $\text{InVO}_4/\text{CoAl}$ -LDH has shown the best morphology, photogenerated carrier separation, and electron/hole transfer, with a high photocurrent response. The production rate of CO was  $174 \mu\text{mol.g}^{-1}$  during 120 min, 9.8 and 2.5 times higher than pure  $\text{InVO}_4$  and  $\text{CoAl}$ -LDH, respectively, with about complete CO selectivity. Indium vanadate has the potential for photocatalytic  $\text{CO}_2$  photoreduction. However, it needs to increase active sites and modify for charge recombination reduction. In a new research,  $\text{InVO}/\text{g-C}_3\text{N}_4$  photocatalysts have been prepared by forming  $\text{InVO}_4$  nanoparticles on  $\text{g-C}_3\text{N}_4$  with nitrogen defects. The modified scheme of  $\text{InVO}/\text{g-C}_3\text{N}_4$  has shown a high reduction efficiency of  $\text{CO}_2$  without a sacrificial agent, with rates 1.8–2.8 folds greater than bare CN and pristine  $\text{InVO}_4$ , which has been attributed to enhanced  $\text{CO}_2$  adsorption and charge carrier separation excited by the Z-scheme heterojunction among CN and  $\text{InVO}_4$  [153]. In pursuit of efforts to develop efficient protocols for the fabrication of  $\text{InVO}_4$  photocatalysts, a direct Z-scheme of 2D  $\text{InVO}_4/\text{Bi}_2\text{WO}_6$  heterojunction has been fabricated through a two-step hydrothermal method [154]. The  $\text{InVO}_4/\text{Bi}_2\text{WO}_6$  composite has a superior photocatalytic capability for the reduction of  $\text{CO}_2$  into CO and  $\text{CH}_4$ , particularly under the visible light spectrum. The CO production rate achieves a maximum value of  $18 \mu\text{mol.g}^{-1}.\text{h}^{-1}$ . In contrast,  $\text{CH}_4$  generation shows a rate of  $1.1 \mu\text{mol.g}^{-1}.\text{h}^{-1}$  surpassing that which is guided by unmodified  $\text{InVO}_4$  and  $\text{Bi}_2\text{WO}_6$  substrates. In another study, an ultrathin nanosheet of  $\text{InVO}_4$  has been initially synthesized, measuring 1.5 nm in thickness. In order to construct a heterojunction photocatalyst based on a step-scheme (S-scheme) configuration, the in-situ deposition of diethylenetriamine (DETA)-modified CdSe has been used over the surface of  $\text{InVO}_4$  nanosheets [155]. The protonated diethylenetriamine serves as an amine bridge, facilitating the creation of a cohesive chemical linkage at the interface between DETA-CdSe/ $\text{InVO}_4$ , consequently supporting the diffusion of carriers at this interface. This photocatalyst has demonstrated a significant CO production rate of  $28 \text{ mmol.g}^{-1}.\text{h}^{-1}$ , which surpasses both DETA-CdSe and  $\text{InVO}_4$  nanosheets. This result suggests the practical applicability of the photocatalyst in photocatalytic  $\text{CO}_2$  reduction reactions. The novel technique of employing interfacial chemical bonding to enhance interfacial charge transfer represents a highly promising approach toward enhancing photocatalytic performance. In another research,  $\text{InVO}_4$  with oxygen vacancy through the in-situ growth on  $\text{C}_3\text{N}_4$  (2D) has been prepared by  $\text{HNO}_3$  for effective  $\text{CO}_2$  reduction [156]. The triple role of  $\text{HNO}_3$  involves protonating  $\text{C}_3\text{N}_4$  (p- $\text{C}_3\text{N}_4$ ), facilitating the growth of  $\text{InVO}_4$  on  $\text{C}_3\text{N}_4$ , and helping to form oxygen vacancies. These effects facilitate the process of interfacial charge transfer via the S-scheme junction. Moreover, the introduction of protonated  $\text{C}_3\text{N}_4$  brings about notable enhancements in electrical conductivity, stimulates the activity of  $\text{CO}_2$ , and facilitates the transformation into products. In another similar study, the synthesis of a novel S-scheme utilizing 0D/2D heterostructures consisting of  $\text{InVO}_4$  quantum dots (QDs) and  $\text{g-C}_3\text{N}_4$  ultrathin nanosheets have been investigated to

achieve improved efficiency for photocatalytic reduction of  $\text{CO}_2$ . The Density Functional Theory (DFT) indicates that the creation of an  $\text{InVO}_4/\text{g-C}_3\text{N}_4$  heterostructure could potentially improve the adsorption and activation of  $\text{CO}_2$ . Furthermore, the 0D/2D structure can effectively stabilize the  $\text{COOH}^*$  intermediates and facilitate rapid CO desorption [157].

MXenes, a new family of 2D materials, have recently attracted consideration as a promising substitute for noble metal co-catalyst owing to their cost-efficiency, unique layered system, and perfect electrical, optical, and thermodynamic properties [158, 159]. As a result of these characteristics, Li et al. have synthesized a 3D heterosystem in the form of a hydrangea-like structure, comprising  $\text{InVO}_4$  and  $\text{Ti}_3\text{C}_2\text{T}_x$  [160]. The optimized proportion of  $\text{Ti}_3\text{C}_2\text{T}_x/\text{InVO}_4$  is employed in the preparation of photocatalysts to form hierarchical conjunction architecture with 2D/2D surface interaction. The  $\text{InVO}_4/\text{Ti}_3\text{C}_2\text{T}_x$  composite material has exhibited superior photon trapping performance and heightened accessibility to reactive sites, which can be attributed to the augmented BET-specific surface areas. Furthermore, this composite is evidenced to possess a remarkably enhanced  $\text{CO}_2$  adsorption capacity that is synergistically correlated with the fundamental feature of  $\text{Ti}_3\text{C}_2\text{T}_x$ .

Another group of vanadate compounds is  $\text{ZnV}_2\text{O}_6$ , which could be modified by proton-rich functionalized  $\text{C}_3\text{N}_4$  (f- $\text{C}_3\text{N}_4$ ) to increase converting  $\text{CO}_2$  in liquid form [161]. The f- $\text{C}_3\text{N}_4/\text{ZnV}_2\text{O}_6$  composite exhibits superior performance in converting  $\text{CO}_2$  through photosynthesis when NaOH solution is a reducing agent compared to utilizing  $\text{H}_2\text{O}$  or  $\text{KHCO}_3$  solutions in the photoreactor. The modification of  $\text{ZnV}_2\text{O}_6$  with f- $\text{C}_3\text{N}_4$  in a 1:1 ratio results in the most significant production of  $\text{CH}_3\text{OH}$ . The  $\text{ZnV}_2\text{O}_6/\text{f-C}_3\text{N}_4$  (1:1) nanosheets show a  $\text{CH}_3\text{OH}$  generation rate of  $4665.6 \mu\text{mole.g}^{-1}$  under HID Xe lamp, which is 1.25 times higher than the production rate of  $3742.1 \mu\text{mole.g}^{-1}$  achieved in a solar photoreactor (Fig. 13). The efficacy of photocatalytic  $\text{CO}_2$  conversion is found to be notably higher in the externally reflected photoreactor than in the solar photoreactor due to its high capacity for light absorption. According to band energy theory, if the reduction potential of the reaction is lower than the CB potential of the semiconductor, the photoinduced electrons can consume efficiently [162]. The boosted productivity of externally reflected photoreactors can be attributed to the reflector's ability to increase photon flux, which ultimately facilitates  $\text{CO}_2$  reduction. Another composition is  $\text{V}_2\text{O}_5$  hybridized with  $\text{ZnV}_2\text{O}_6$  via a two-step hydrothermal method to convert  $\text{CO}_2$  [163]. The  $\text{ZnV}_2\text{O}_6/\text{V}_2\text{O}_5$  nanosheets display good electrochemical properties at the optimized temperature of the calcination process, which produces carbon monoxide by 1.9 and 2.2 times higher compared to  $\text{ZnV}_2\text{O}_6$  and  $\text{V}_2\text{O}_5$ .

## 5. Conclusions

Recently, significant advancements in research pertaining to vanadate photocatalysts have been documented and emphasized. Therefore, a comparative study is reviewed on vanadate composites for high performance in photocatalytic applications. Thus, this review discussed in detail the following:

- **Synthesis methods of vanadate compounds preparation:** various preparation processes such as solvo/hydrothermal, self-assembly procedure, precipitation route, sol-gel technique, ultrasound-assisted, and solid-state reaction methods to synthesize vanadate nanocomposites with diverse morphologies with the advantages and disadvantages of each method were presented.

- **Approaches for enhancing light absorption of vanadate semiconductor:** Numerous approaches, including energy band engineering, catalyst conjunction, heterojunction structure, doping, and surface moderating, have been employed to enhance light absorptivity, modify charge carrier dynamics, improve photocatalytic durability, and accelerate surface reaction kinetics. These include but are not limited to doped-BiVO<sub>4</sub>, Z-scheme BiVO<sub>4</sub>, heterojunction BiVO<sub>4</sub>, InVO<sub>4</sub>, FeVO<sub>4</sub> heterostructure, Ag<sub>3</sub>VO<sub>4</sub>, and VO<sub>4</sub>-based binary and ternary composites.

**Photocatalytic applications of decorated vanadate compounds:** the modified photocatalysts exhibit considerable potential for various applications, including hydrogen production by water splitting, pollutant degradation, water treatment, CO<sub>2</sub>, and heavy metals reduction. Improving the efficacy of photocatalysis can be achieved by mitigating the recombination of electron-hole pairs and increasing the proficiency of electron transmission. In general, defect-rich 2D systems and 3D nanotubes exhibit these desirable characteristics. For instance, in the case of hydrogen production, the outcomes revealed that the heterojunction Z-scheme configuration exhibits superior performance compared to other microstructures. Furthermore, the application of a 2D-1D BiVO<sub>4</sub>/CdS heterostructure photocatalyst enhances by 40 times the H<sub>2</sub> production from benzyl alcohol than pure BiVO<sub>4</sub>. On the other hand, in CO<sub>2</sub> reduction, the CO production rate can reach a relatively high value (18 μmol.g<sup>-1</sup>.h<sup>-1</sup>) when InVO<sub>4</sub>/Bi<sub>2</sub>WO<sub>6</sub> composite is used. Furthermore, a 90% removal of heavy metals and 100% of organic pollutants is attained when BiVO<sub>4</sub>/rGO/g-C<sub>3</sub>N<sub>4</sub> and Montmorillonite/BiVO<sub>4</sub> structures were used, respectively. Finally, a majority of photocatalysts exhibit reactivity solely towards ultraviolet radiation in the facilitation of water splitting. The development of photocatalysts that respond effectively to visible light is of great significance to enhance the utilization of solar energy. Additional investigation is warranted to develop binary and ternary composite materials capable of light absorption in the visible spectrum and enhancing degradation efficacy by reducing electron recombination with decreased catalyst utilization and timeframe. Subsequently, novel prospects emerge for effectively tackling challenges via the utilization of altered composites. The diminution of catalytic efficacy over an extended time frame constitutes a commonly encountered predicament for all photocatalysts, thereby posing a significant impediment to their commercial or industrial utilization. The principal predicament pertains to the amalgamation of a vast, high-functioning vanadate photocatalyst that exhibits impeccable photocatalytic prowess. The implementation of a novel approach involving the manufacturing of vanadium-centered substances with atomic-thin dimensions, or the transformation of nanosheets into single-layer entities via delamination, represents a promising approach for actual development.

### CRedit authorship contribution statement

**Mehrdad Mirzaei:** Writing – original draft, Resources.

**Asieh Akhoondi:** Writing – original draft, Supervision.

**Wael Hamd:** Writing – review & editing.

**Jorge Noé Díaz de León:** Writing – review & editing.

**Rengaraj Selvaraj:** Writing – review & editing.

### Data availability

As this is a review article, no new data were generated. All information is publicly available or cited appropriately within the article.

### Declaration of competing interest

This research received no external funding. The authors have no acknowledgments to declare.

### Funding and acknowledgment

This research received no external funding.

### References

- [1] M. Yang, G. Ma, H. Yang, Z. Xiaoqiang, W. Yang, H. Hou, Advanced strategies for promoting the photocatalytic performance of FeVO<sub>4</sub> based photocatalysts: A review of recent progress, *J. Alloys Compd.* 941 (2023) 168995. <https://doi.org/10.1016/j.jallcom.2023.168995>.
- [2] G.-Q. Zhao, X. Long, J. Zou, J. Hu, F.-P. Jiao, Design of hollow nanostructured photocatalysts for clean energy production, *Coord. Chem. Rev.* 477 (2023) 214953. <https://doi.org/10.1016/j.ccr.2022.214953>.
- [3] R. Yang, Y. Zhang, Y. Fan, R. Wang, R. Zhu, et al., InVO<sub>4</sub>-based photocatalysts for energy and environmental applications, *Chem. Eng. J.* 428 (2022) 131145. <https://doi.org/10.1016/j.cej.2021.131145>.
- [4] A. Akhoondi, A.I. Osman, A.A. Eslami, Direct catalytic production of dimethyl ether from CO and CO<sub>2</sub>: A review, *Synth. Sinter.* 1 (2021) 105–120. <https://doi.org/10.53063/synsint.2021.1229>.
- [5] Q. Jia, A. Iwase, A. Kudo, BiVO<sub>4</sub>-Ru/SrTiO<sub>3</sub>:Rh composite Z-scheme photocatalyst for solar water splitting, *Chem. Sci.* 5 (2014) 1513. <https://doi.org/10.1039/C3SC52810C>.
- [6] H.Y. Lin, Y. Chen, Y. Chen, Water splitting reaction on NiO/InVO<sub>4</sub> under visible light irradiation, *Int. J. Hydrog. Energy.* 32 (2007) 86–92. <https://doi.org/10.1016/j.ijhydene.2006.04.007>.
- [7] W. Hamd, S. Cobo, J. Fize, G. Baldinozzi, W. Schwartz, et al., Mesoporous α-Fe<sub>2</sub>O<sub>3</sub> thin films synthesized via the sol–gel process for light-driven water oxidation, *Phys. Chem. Chem. Phys.* 14 (2012) 13224–13232. <https://doi.org/10.1039/C2CP42535A>.
- [8] T. Lv, D. Li, Y. Hong, B. Luo, D. Xu, et al., Facile synthesis of CdS/Bi<sub>4</sub>V<sub>2</sub>O<sub>11</sub> photocatalysts with enhanced visible-light photocatalytic activity for degradation of organic pollutants in water, *Dalton Trans.* 46 (2017) 12675–12682. <https://doi.org/10.1039/C7DT02151H>.
- [9] N. Tian, H. Huang, Y. He, Y. Guo, T. Zhang, Y. Zhang, Mediator-free direct Z-scheme photocatalytic system: BiVO<sub>4</sub>/g-C<sub>3</sub>N<sub>4</sub> organic–inorganic hybrid photocatalyst with highly efficient visible-light-induced photocatalytic activity, *Dalton Trans.* 44 (2015) 4297–4307. <https://doi.org/10.1039/C4DT03905J>.
- [10] W. Shi, Y. Yan, X. Yan, Microwave-assisted synthesis of nano-scale BiVO<sub>4</sub> photocatalysts and their excellent visible-light-driven photocatalytic activity for the degradation of ciprofloxacin, *Chem. Eng. J.* 215–216 (2013) 740–746. <https://doi.org/10.1016/j.cej.2012.10.071>.
- [11] A. Akhoondi, U. Feleni, B. Bethi, A.O. Idris, A. Hojjati-Najafabadi, Advances in metal-based vanadate compound photocatalysts: synthesis, properties and applications, *Synth. Sinter.* 1 (2021) 151–168. <https://doi.org/10.53063/synsint.2021.1344>.
- [12] B.C.B. Salgado, R.A. Cardeal, A. Valentini, Photocatalysis and photodegradation of pollutants, nanomaterials applications for environmental matrices, Elsevier. (2019). <https://doi.org/10.1016/B978-0-12-814829-7.00015-X>.
- [13] A. Malathi, J. Madhavan, M. Ashokkumar, P. Arunachalam, A review on BiVO<sub>4</sub> photocatalyst: Activity enhancement methods for solar photocatalytic applications, *Appl. Catal. A.* 555 (2018) 47–74. <https://doi.org/10.1016/j.apcata.2018.02.010>.
- [14] P. Dhull, A. Sudhaik, V. Sharma, P. Raizada, V. Hasija, et al., An overview on InVO<sub>4</sub>-based photocatalysts: Electronic properties, synthesis, enhancement strategies, and photocatalytic applications,



- Mol. Catal. 539 (2023) 113013. <https://doi.org/10.1016/j.mcat.2023.113013>.
- [15] L. Zhang, H.H. Mohamed, R. Dillert, D. Bahnemann, Kinetics and mechanisms of charge transfer processes in photocatalytic systems: A review, *J. Photochem. Photobiol. C* 13 (2012) 263–276. <https://doi.org/10.1016/j.jphotochemrev.2012.07.002>.
- [16] Q. Han, Advances in preparation methods of bismuth-based photocatalysts, *Chem. Eng. J.* 414 (2021) 127877. <https://doi.org/10.1016/j.cej.2020.127877>.
- [17] M.S. Shruti, S. Khilari, E.J.J. Samuel, H. Han, A.K. Nayak, Recent trends in graphene assisted vanadium based nanocomposites for supercapacitor applications, *J. Energy Storage* 63 (2023) 107006. <https://doi.org/10.1016/j.est.2023.107006>.
- [18] D.T.T. Trinh, W. Khanitchaidecha, D. Channei, A. Nakaruk, Synthesis, characterization and environmental applications of bismuth vanadate, *Res. Chem. Intermed.* 45 (2019) 5217–5259. <https://doi.org/10.1007/s11164-019-03912-2>.
- [19] E. Suvaci, E. Özel, Hydrothermal Synthesis, *Encyclopedia of Materials: Technical Ceramics and Glasses*, Elsevier, 1 (2021) 59–68. <https://doi.org/10.1016/B978-0-12-803581-8.12096-X>.
- [20] S.-H. Feng, G.-H. Li, Hydrothermal and solvothermal syntheses, modern inorganic synthetic chemistry (2nd Edition), Elsevier, (2017) 73–104. <https://doi.org/10.1016/B978-0-444-63591-4.00004-5>.
- [21] H.K. Lin, T.-H. Yan, S. Bashir, J.L. Liu, Synthesis of nanomaterials using bottom-up methods, *Advanced Nanomaterials and Their Applications in Renewable Energy* (Second Edition), Elsevier, (2022) 61–110. <https://doi.org/10.1016/B978-0-323-99877-2.00003-5>.
- [22] D. Nunes, A. Pimentel, L. Santos, P. Barquinha, L. Pereira, et al., Synthesis, design, and morphology of metal oxide nanostructures, Elsevier, (2019) 21–57. <https://doi.org/10.1016/B978-0-12-811512-1.00002-3>.
- [23] N.S. Bajaj, R.A. Joshi, Energy materials: synthesis and characterization techniques, *Energy Materials*, Elsevier, (2021) 61–82. <https://doi.org/10.1016/B978-0-12-823710-6.00019-4>.
- [24] A.V. Rane, K. Kanny, V.K. Abitha, S. Thomas, Methods for Synthesis of Nanoparticles and Fabrication of Nanocomposites, *Synthesis of Inorganic Nanomaterials*, Elsevier, (2018) 121–139. <https://doi.org/10.1016/B978-0-08-101975-7.00005-1>.
- [25] M.M. Ahmad, S. Mushtaq, H.S. Al Qahtani, A. Sedky, M.W. Alam, Investigation of TiO<sub>2</sub> Nanoparticles Synthesized by Sol-Gel Method for Effectual Photodegradation, Oxidation and Reduction Reaction, *Crystals* 11 (2021) 1456. <https://doi.org/10.3390/cryst11121456>.
- [26] J.G. Mahy, L. Lejeune, T. Haynes, S.D. Lambert, R.H.M. Marcilli, et al., Eco-Friendly Colloidal Aqueous Sol-Gel Process for TiO<sub>2</sub> Synthesis: The Peptization Method to Obtain Crystalline and Photoactive Materials at Low Temperature, *Catalysts* 11 (2021) 768. <https://doi.org/10.3390/catal11070768>.
- [27] A. Akhoondi, M. Ziarati, N. Khandan, Hydrothermal Production of Highly Pure Nano Pyrite in a Stirred Reactor, *Iran J. Chem. Chem. Eng.* 33 (2014) 15–19. <https://doi.org/10.30492/IJCE.2014.7189>.
- [28] B.P. Kafle, Introduction to nanomaterials and application of UV–Visible spectroscopy for their characterization, *Chemical Analysis and Material Characterization by Spectrophotometry*, Elsevier, (2020) 147–198. <https://doi.org/10.1016/B978-0-12-814866-2.00006-3>.
- [29] Q. Zhang, L. Gao, Preparation of oxide nanocrystals with tunable morphologies by the moderate hydrothermal method: insights from rutile TiO<sub>2</sub>, *Langmuir* 19 (2003) 967–971. <https://doi.org/10.1021/la020310q>.
- [30] A. Akhoondi, M. Aghaziarati, N. Khandan, Production of highly pure iron disulfide nanoparticles using hydrothermal synthesis method, *Appl. Nanosci.* 3 (2013) 417–422. <https://doi.org/10.1007/s13204-012-0153-1>.
- [31] Y.X. Gan, A.H. Jayatissa, Z. Yu, X. Chen, M. Li, Hydrothermal Synthesis of Nanomaterials, *J. Nanomater.* 2020 (2020) 8917013. <https://doi.org/10.1155/2020/8917013>.
- [32] R.L. Naik, T.B. Narsaiah, Hydrothermal synthesis and characterization of nanocrystalline zinc vanadate (Zn<sub>2</sub>V<sub>2</sub>O<sub>7</sub>) on graphene oxide scaffolds, *Mater. Today: Proc.* 72 (2023) 268–273. <https://doi.org/10.1016/j.matpr.2022.07.266>.
- [33] K. Sekar, A. Kassam, Y. Bai, B. Coulson, W. Li, et al., Hierarchical bismuth vanadate/reduced graphene oxide composite photocatalyst for hydrogen evolution and bisphenol A degradation, *Appl. Mater. Today* 22 (2021) 100963. <https://doi.org/10.1016/j.apmt.2021.100963>.
- [34] A. Akhoondi, M. Aghaziarati, N. Khandan, Hydrothermal production of nano pyrite, *1st Int. Region. Chem. Petrol. Eng.* (2010).
- [35] X. Cao, Y. Gu, Y. Fang, D. Johnson, C. Chen, et al., Self-assembled BiVO<sub>4</sub> mesocrystals for efficient photocatalytic decontamination of microcystin-LR, *Environ. Chem. Lett.* 20 (2022) 1595–1601. <https://doi.org/10.1007/s10311-022-01426-9>.
- [36] G.Q. Tan, C. Xu, H.J. Ren, W. Yang, C.C. Zhao, A. Xia, Synthesis and Photocatalytic Activities of Bamboo-Like FeVO<sub>4</sub> Nanocrystalline, *J. Nano Res.* 46 (2017) 123–134. <https://doi.org/10.4028/www.scientific.net/JNanoR.46.123>.
- [37] A. Akhoondi, M. Aghaziarati, N. Khandan, Thermal Treatment on Synthesized Nano Pyrite, *NTC2011* (2011).
- [38] Z. Li, Z. Bao, F. Yao, H. Cao, J. Wang, et al., One-dimensional bismuth vanadate nanostructures constructed Z-scheme photocatalyst for highly efficient degradation of antibiotics, *J. Water Process. Eng.* 46 (2022) 102599. <https://doi.org/10.1016/j.jwpe.2022.102599>.
- [39] Y. Lin, H. Chi, J. Lin, F. Chen, C. Chen, C. Lu, Eight crystalline phases of bismuth vanadate by controllable hydrothermal synthesis exhibiting visible-light-driven photocatalytic activity, *Mol. Catal.* 506 (2021) 111547. <https://doi.org/10.1016/j.mcat.2021.111547>.
- [40] A. Akhoondi, M. Aghaziarati, N. Khandan, Nano pyrite production by hydrothermal method and marcasite removal using sodium bicarbonate, *Nanotechnology Iranian Student Conference*, (2012).
- [41] M.M. Sajid, H. Zhai, N.A. Shad, M. Shafique, A.M. Afzal, et al., Photocatalytic performance of ferric vanadate (FeVO<sub>4</sub>) nanoparticles synthesized by hydrothermal method, *Mater. Sci. Semicond. Process.* 129 (2021) 105785. <https://doi.org/10.1016/j.mssp.2021.105785>.
- [42] F.-L. Zeng, H.-L. Zhu, R.-N. Wang, X.-Y. Yuan, K. Sun, et al., Bismuth vanadate: A versatile heterogeneous catalyst for photocatalytic functionalization of C(sp<sup>2</sup>)–H bonds, *Chin. J. Catal.* 46 (2023) 157–166. [https://doi.org/10.1016/S1872-2067\(23\)64391-8](https://doi.org/10.1016/S1872-2067(23)64391-8).
- [43] S.S. Basu, S. Rahut, A.S. Bisht, J.K. Basu, Surfactant-assisted tuning of K<sub>2</sub>V<sub>3</sub>O<sub>8</sub> nanorods for robust charge dynamics in semiconductor photocatalysis, *Mater. Sci. Semicond. Process.* 147 (2022) 106681. <https://doi.org/10.1016/j.mssp.2022.106681>.
- [44] T. Zhang, H. Li, X. Tang, J. Zhong, J. Li, et al., Boosted photocatalytic performance of OV-rich BiVO<sub>4</sub> hollow microsphere self-assembled with the assistance of SDBS, *J. Colloid Interface Sci.* 634 (2023) 874–886. <https://doi.org/10.1016/j.jcis.2022.12.057>.
- [45] M.M. Sajid, H. Assaedi, H. Zhai, Transition metal vanadates (MVO; M=Bi, Fe, Zn) synthesized by a hydrothermal method for efficient photocatalysis, *J. Mater. Sci.: Mater. Electron.* 34 (2023) 539. <https://doi.org/10.1007/s10854-023-09923-5>.
- [46] R. Huo, X. Yang, J. Yang, S. Yang, Y. Xu, Self-assembly synthesis of BiVO<sub>4</sub>/Polydopamine/g-C<sub>3</sub>N<sub>4</sub> with enhanced visible light photocatalytic performance, *Mater. Res. Bull.* 98 (2018) 225–230. <https://doi.org/10.1016/j.materresbull.2017.10.016>.
- [47] Y. Deng, H. Zhou, Y. Zhao, B. Yang, M. Shi, et al., Spatial Separation of Photogenerated Charges on Well-Defined Bismuth Vanadate Square Nanocrystals, *Small* 18 (2022) 2103245. <https://doi.org/10.1002/smll.202103245>.
- [48] Y. Xing, X. Lu, Y. Li, B. Yang, Y. Huang, et al., Self-assembled Ag<sub>4</sub>V<sub>2</sub>O<sub>7</sub>/Ag<sub>3</sub>VO<sub>4</sub> Z-scheme heterojunction by pH adjustment with efficient photocatalytic performance, *J. Adv. Ceram.* 11 (2022) 1789–1800. <https://doi.org/10.1007/s40145-022-0648-5>.
- [49] W. Zhao, Y. Feng, H. Huang, P. Zhou, J. Li, et al., A novel Z-scheme Ag<sub>3</sub>VO<sub>4</sub>/BiVO<sub>4</sub> heterojunction photocatalyst: Study on the excellent photocatalytic performance and photocatalytic mechanism, *Appl. Catal. B: Environ.* 245 (2019) 448–458. <https://doi.org/10.1016/j.apcatb.2019.01.001>.



- [50] Q. Wang, J. Li, L. Xiao, Y. Wang, H. Du, Constructing Z-scheme  $\text{Fe}_3\text{N}/\text{BiVO}_4$  heterojunction via electrostatic self-assembly toward high visible-light photocatalytic hydrogen evolution, *J. Alloys Compd.* 935 (2023) 168062. <https://doi.org/10.1016/j.jallcom.2022.168062>.
- [51] L. Xiao, L. Lin, J. Song, Z. Zhang, X. Wang, W. Su, Construction of a direct Z-scheme  $\text{InVO}_4/\text{La}_2\text{Ti}_2\text{O}_7$  photocatalyst toward efficient and selective  $\text{CO}_2$  reduction to CO, *J. Alloys Compd.* 935 (2023) 168086. <https://doi.org/10.1016/j.jallcom.2022.168086>.
- [52] W. Lou, L. Wang, S. Dong, Z. Cao, J. Sun, Y. Zhang, A facility synthesis of bismuth-iron bimetal MOF composite silver vanadate applied to visible light photocatalysis, *Opt. Mater.* 126 (2022) 112168. <https://doi.org/10.1016/j.optmat.2022.112168>.
- [53] N. Ghazkoob, M. Zargar Shoushtari, I. Kazeminezhad, S.M. Lari Baghal, Investigation of structural, magnetic, optical and photocatalytic properties of zinc ferrite nanowires/bismuth vanadate composite, *J. Alloys Compd.* 900 (2022) 163467. <https://doi.org/10.1016/j.jallcom.2021.163467>.
- [54] A. Zonarsaghar, M. Mousavi-Kamazani, S. Zinatloo-Ajabshir, Co-precipitation synthesis of  $\text{CeVO}_4$  nanoparticles for electrochemical hydrogen storage, *J. Mater. Sci. Mater. Electron.* 33 (2022) 6549–6554. <https://doi.org/10.1007/s10854-022-07829-2>.
- [55] M. Iqbal, M.Z. Ahmad, K. Qureshi, I.A. Bhatti, N. Alwadai, H.S. Kusuma, Template free zinc vanadate flower synthesis, characterization and efficiency for cetirizine-dihydrochloride degradation under UV light irradiation, *Mater. Chem. Phys.* 272 (2021) 124968. <https://doi.org/10.1016/j.matchemphys.2021.124968>.
- [56] N. Ghazkoob, M. Zargar, I. Kazeminejad, S.M. Lari, Synthesis of  $\text{BiVO}_4$  nanoparticles by the co-precipitation method and study the crystal structure, optical and photocatalytic properties of them, *Iran. J. Crystallogr. Mineral.* 28 (2020) 797–806. <https://doi.org/10.29252/ijcm.28.3.797>.
- [57] W. Guo, P. Yu, H. Luo, J. Chi, Z. Jiang, et al., Unveiling the role of surface heterostructure in  $\text{Bi}_0.5\text{Y}_0.5\text{VO}_4$  solid solution for photocatalytic overall water splitting, *J. Catal.* 406 (2022) 193–205. <https://doi.org/10.1016/j.jcat.2022.01.011>.
- [58] S. Wang, L. Zhao, L. Gao, D. Yang, S. Wen, et al., Fabrication of ternary dual Z-Scheme  $\text{AgI}/\text{ZnIn}_2\text{S}_4/\text{BiVO}_4$  heterojunction photocatalyst with enhanced photocatalytic degradation of tetracycline under visible light, *Arab. J. Chem.* 15 (2022) 104159. <https://doi.org/10.1016/j.arabjc.2022.104159>.
- [59] A. Karami, R. Monsef, M.R. Shihan, L.Y. Qassem, M.W. Falah, M. Salavati-Niasari, UV-light-induced photocatalytic response of Pechini sol–gel synthesized erbium vanadate nanostructures toward degradation of colored pollutants, *Environ. Technol. Innov.* 28 (2022) 102947. <https://doi.org/10.1016/j.eti.2022.102947>.
- [60] Y. Feng, C. Jia, H. Zhao, K. Wang, X.-T. Wang, Phase-dependent photocatalytic selective oxidation of cyclohexane over copper vanadates, *New J. Chem.* 46 (2022) 4082–4089. <https://doi.org/10.1039/D1NJ05677H>.
- [61] N.R. Aswathy, J. Varghese, R. Vinod Kumar, Photocatalytic degradation of malachite green using vanadium pentoxide-doped  $\text{NiO}$  thin film by sol–gel spin coating, *Eur. Phys. J. Plus.* 137 (2022) 1344. <https://doi.org/10.1140/epjp/s13360-022-03559-w>.
- [62] K. Anwar, F.K. Naqvi, S. Beg, Synthesis of tetragonally stabilized lanthanum doped bismuth vanadium oxide nanoparticles and its enhanced visible light induced photocatalytic performance, *Phase Transit.* 95 (2022) 64–79. <https://doi.org/10.1080/01411594.2021.2012175>.
- [63] S.A. El-Hakam, F.T. AlShorifi, R.S. Salama, S. Gamal, W.S. Abo El-Yazeed, et al., Application of nanostructured mesoporous silica/bismuth vanadate composite catalysts for the degradation of methylene blue and brilliant green, *J. Mater. Res. Technol.* 18 (2022) 1963–1976. <https://doi.org/10.1016/j.jmrt.2022.03.067>.
- [64] D. Karthigaimuthu, S. Ramasundaram, P. Nisha, B.A. Kumar, J. Sriram, et al., Synthesis of  $\text{MoS}_2/\text{Mg}(\text{OH})_2/\text{BiVO}_4$  hybrid photocatalyst by ultrasonic homogenization assisted hydrothermal methods and its application as sunlight active photocatalyst for water decontamination, *Chemosphere.* 308 (2022) 136406. <https://doi.org/10.1016/j.chemosphere.2022.136406>.
- [65] V. Thirupugazhmani, S. Shameena, K. Thirumalai, A. Ravi, P.A. Vivekanand, et al., Ultrasonic assisted synthesis of RGO supported  $\text{HoVO}_4\text{-ZnO}$  nanocomposites, their enhanced photocatalytic activities and Rhodamine B degradation, *Environ. Res.* 214 (2022) 113743. <https://doi.org/10.1016/j.envres.2022.113743>.
- [66] H.Q. Alijani, S. Irvani, R.S. Varma, Bismuth vanadate ( $\text{BiVO}_4$ ) nanostructures: eco-friendly synthesis and their photocatalytic applications, *Catalysts.* 13 (2023) 59. <https://doi.org/10.3390/catal13010059>.
- [67] A. Ansari, D. Mohanta, Structural and XPS studies of polyhedral europium doped gadolinium orthovanadate ( $\text{Eu}^{3+}:\text{GdVO}_4$ ) nanocatalyst for augmented photodegradation against Congo-red, *Phys. E: Low-Dimens. Syst. Nanostruct.* 143 (2022) 115357. <https://doi.org/10.1016/j.physe.2022.115357>.
- [68] Y. Chen, Y. Zhang, W. Wang, X. Xu, Y. Li, et al., Bandgap Engineering and Oxygen Vacancies of  $\text{Ni}_x\text{V}_2\text{O}_{5+x}$  ( $x = 1, 2, 3$ ) for Efficient Visible Light-Driven  $\text{CO}_2$  to CO with Nearly 100% Selectivity, *Sol. RRL.* 6 (2022) 2200099. <https://doi.org/10.1002/solr.202200099>.
- [69] X. Jin, R. Wang, Y. Zhou, J. Lai, J. Li, et al., A comprehensive experimental and first-principles study on magnesium-vanadium oxides, *J. Alloys Compd.* 896 (2022) 162862. <https://doi.org/10.1016/j.jallcom.2021.162862>.
- [70] S.S. Patil, J. Lee, T. Kim, L.R. Nagappagari, K. Lee, Controlled synthesis and structural modulation to boost intrinsic photocatalytic activity of  $\text{BiVO}_4$ , *CrystEngComm.* 24 (2022) 2686. <https://doi.org/10.1039/D1CE01700D>.
- [71] I.A. Mkhaliid, R.M. Mohamed, M. Alhaddad, A. Basaleh, L.A. Al-Hajji, A.A. Ismail, Construction of mesoporous lanthanum orthovanadate/carbon nitride heterojunction photocatalyst for the mineralization of trichloroethylene, *Ceram. Int.* 48 (2022) 14899–14912. <https://doi.org/10.1016/j.ceramint.2022.02.028>.
- [72] T. Du, M. Cui, Y. Chao, Y. Xiao, Z. Ren, et al., Preparation and photocatalytic properties of highly dispersed samarium vanadate nanoparticles supported on H-mordenite composites by template-free method, *J. Photochem. Photobiol. A.* 433 (2022) 114207. <https://doi.org/10.1016/j.jphotochem.2022.114207>.
- [73] I.B. Elizabeth, E. Elanthamilan, S.-F. Wang, I.S. Lydia, Facile synthesis of multifunctional zinc vanadate/polyaniline composite for photocatalytic degradation and supercapacitor applications, *Chemosphere.* 307 (2022) 136123. <https://doi.org/10.1016/j.chemosphere.2022.136123>.
- [74] M. Nadolska, M. Szkoda, K. Trzcinski, P. Niedzialkowski, J. Ryl, et al., Insight into Potassium Vanadates as Visible-Light-Driven Photocatalysts: Synthesis of V(IV)-Rich Nano/Microstructures for the Photodegradation of Methylene Blue, *Inorg. Chem.* 61 (2022) 9433–9444. <https://doi.org/10.1021/acs.inorgchem.2c00136>.
- [75] J. Huang, Y. Ma, Q. Chen, J. Zhu, H. Jiang, et al., Effect of water-oil ratio on the photocatalytic performance of visible light-active  $\text{BiVO}_4$  nanoparticles prepared by inverse microemulsion-calcination method, *Chemosphere.* 299 (2022) 134454. <https://doi.org/10.1016/j.chemosphere.2022.134454>.
- [76] S. Bakhtiarnia, S. Sheibani, A. Billard, E. Aubry, M. Arab, Deposition of nanoporous  $\text{BiVO}_4$  thin-film photocatalyst by reactive magnetron sputtering: Effect of total pressure and substrate, *Trans. Nonferrous Met. Soc. China.* 32 (2022) 957–971. [https://doi.org/10.1016/S1003-6326\(22\)65846-1](https://doi.org/10.1016/S1003-6326(22)65846-1).
- [77] R.D. Tentu, S. Basu, Photocatalytic water splitting for hydrogen production, *Curr. Opin. Electrochem.* 5 (2017) 56–62. <https://doi.org/10.1016/j.coelec.2017.10.019>.
- [78] X. Zhong, Y. Li, H. Wu, R. Xie, Recent progress in  $\text{BiVO}_4$ -based heterojunction nanomaterials for photocatalytic applications, *Mater. Sci. Eng. B.* 289 (2023) 116278. <https://doi.org/10.1016/j.mseb.2023.116278>.

- [79] P. Bai, P. Wang, Y. Wu, X. Pang, M. Song, et al., Junction of  $\text{ZnIn}_2\text{S}_3$  and bismuth vanadate as Z-scheme photocatalyst for enhanced hydrogen evolution activity: The role of interfacial interactions, *J. Colloid Interface Sci.* 628 (2022) 488–499. <https://doi.org/10.1016/j.jcis.2022.08.078>.
- [80] F.-K. Shang, M.-Y. Qi, C.-L. Tan, Z.-R. Tang, Y.-J. Xu, Nanoscale Assembly of  $\text{CdS}/\text{BiVO}_4$  Hybrids for Coupling Selective Fine Chemical Synthesis and Hydrogen Production under Visible Light, *ACS Phys. Chem. Au.* 2 (2022) 216–224. <https://doi.org/10.1021/acspchemau.1c00053>.
- [81] Y. Fan, R. Yang, R. Zhu, Z. Zhu,  $\text{CdS}$  decorated artificial leaf  $\text{BiVO}_4/\text{InVO}_4$  for photocatalytic hydrogen production and simultaneous degradation of biological hydrogen production wastewater, *Catal. Today.* 364 (2021) 190–195. <https://doi.org/10.1016/j.cattod.2020.04.012>.
- [82] M. Imran, A.B. Yousaf, M. Farooq, P. Kasak, Enhancement of visible light-driven hydrogen production over zinc cadmium sulfide nanoparticles anchored on  $\text{BiVO}_4$  nanorods, *Int. J. Hydrog. Energy.* 47 (2022) 8327–8337. <https://doi.org/10.1016/j.ijhydene.2021.12.193>.
- [83] K. Manikantan, K. Shanmugasundaram, P. Thirunavukkarasu, Enhanced photocatalytic dye degradation and hydrogen evolution performance of  $\text{Cu}$  encapsulated  $\text{BiVO}_4$  under visible light irradiation, *Chem. Phys. Impact.* 6 (2023) 100178. <https://doi.org/10.1016/j.chphi.2023.100178>.
- [84] S. Yue, W. Hu, J. Wang, M. Sun, Z. Huang, et al., Dramatically promoted photocatalytic water splitting over  $\text{InVO}_4$  via extending hole diffusion length by surface polarization, *Chem. Eng. J.* 435 (2022) 135005. <https://doi.org/10.1016/j.cej.2022.135005>.
- [85] A. Akhoondi, H. Ghaebi, L. Karuppasamy, M.M. Rahman, P. Sathishkumar, Recent advances in hydrogen production using MXenes-based metal sulfide photocatalysts, *Synth. Sinter.* 2 (2022) 37–54. <https://doi.org/10.53063/synsint.2022.21106>.
- [86] Y. Li, Y. Liu, D. Xing, J. Wang, L. Zheng, et al., 2D/2D heterostructure of ultrathin  $\text{BiVO}_4/\text{Ti}_3\text{C}_2$  nanosheets for photocatalytic overall Water splitting, *Appl. Catal. B.* 285 (2021) 119855. <https://doi.org/10.1016/j.apcatb.2020.119855>.
- [87] W. Wang, M. Chi, X.Y. Zhang, I.N. Ivafov, Z. Bao, et al., Construction of 2D  $\text{BiVO}_4\text{--CdS--Ti}_3\text{C}_2\text{Tx}$  Heterostructures for Enhanced Photo-redox Activities, *ChemCatChem.* 12 (2020) 3496–3503. <https://doi.org/10.1002/cctc.202000448>.
- [88] X. Du, T. Zhao, X. Xiu, Z. Xing, Z. Li, et al.,  $\text{BiVO}_4/\text{ZnIn}_2\text{S}_4/\text{Ti}_3\text{C}_2$  MXene quantum dots assembly all-solid-state direct Z-Scheme photocatalysts for efficient visible-light-driven overall water splitting, *Appl. Mater. Today.* 20 (2020) 100719. <https://doi.org/10.1016/j.apmt.2020.100719>.
- [89] A. Hayat, M. Sohail, T.A. Taha, S. Kumar, A.G. Al-Sehemi, et al., Synergetic effect of bismuth vanadate over copolymerized carbon nitride composites for highly efficient photocatalytic  $\text{H}_2$  and  $\text{O}_2$  generation, *J. Colloid Interface Sci.* 627 (2022) 621–629. <https://doi.org/10.1016/j.jcis.2022.07.012>.
- [90] H.Y. Hafeez, S.K. Lakhera, M.V. Shankar, B. Neppolian, Synergetic improvement in charge carrier transport and light harvesting over ternary  $\text{InVO}_4\text{--g-C}_3\text{N}_4/\text{rGO}$  hybrid nanocomposite for hydrogen evolution reaction, *Int. J. Hydrog. Energy.* 45 (2020) 7530–7540. <https://doi.org/10.1016/j.ijhydene.2019.05.235>.
- [91] B. Hu, F. Cai, T. Chen, M. Fan, C. Song, et al., Hydrothermal Synthesis  $\text{g-C}_3\text{N}_4/\text{Nano-InVO}_4$  Nanocomposites and Enhanced Photocatalytic Activity for Hydrogen Production under Visible Light Irradiation, *ACS Appl. Mater. Interfaces.* 7 (2015) 18247–18256. <https://doi.org/10.1021/acsami.5b05715>.
- [92] F.-Y. Chen, L. Cheng, Y.-B. Tang, K.-K. Shu, W.-L. Shi, Construction of Z-scheme heterojunction  $\text{g-C}_3\text{N}_4/\text{CQDs}/\text{InVO}_4$  with broad-spectrum response for efficient rhodamine B degradation and  $\text{H}_2$  evolution under visible light, *Chem. Technol. Biotechnol.* 96 (2021) 3074–3083. <https://doi.org/10.1002/jctb.6859>.
- [93] Y. Fan, R. Yang, R. Zhu, H. Zhao, Q. Lu, et al.,  $\text{CdS}$ -based artificial leaf for photocatalytic hydrogen evolution and simultaneous degradation of biological wastewater, *Chemosphere.* 301 (2022) 134713. <https://doi.org/10.1016/j.chemosphere.2022.134713>.
- [94] H.Y. Hafeez, J. Mohammed, A.B. Suleiman, C.E. Ndikilar, I. Muhammad, R.S. Sa'id, Robust One-Pot Solvothermal Incorporation of  $\text{InVO}_4$  with Polymeric- $\text{C}_3\text{N}_4$  Nanosheets with Improved Charge Carrier Separation and Transfer: A Highly Efficient and Stable Photocatalyst for Solar Fuel ( $\text{H}_2$ ) Generation, SSRN. <http://dx.doi.org/10.2139/ssrn.4217383>.
- [95] A.S. Alkorbi, K.Y. Kumar, M.K. Prashanth, L. Parashuram, A. Abate, et al., Samarium vanadate affixed sulfur self doped  $\text{g-C}_3\text{N}_4$  heterojunction; photocatalytic, photoelectrocatalytic hydrogen evolution and dye degradation, *Int. J. Hydrog. Energy.* 47 (2022) 12988–13003. <https://doi.org/10.1016/j.ijhydene.2022.02.071>.
- [96] S. Sun, R. Gao, X. Liu, L. Pan, C. Shi, et al., Engineering interfacial band bending over bismuth vanadate/carbon nitride by work function regulation for efficient solar-driven water splitting, *Sci. Bull.* 67 (2022) 389–397. <https://doi.org/10.1016/j.scib.2021.10.009>.
- [97] S. Zang, X. Cai, M. Chen, D. Teng, F. Jing, et al., Tunable Carrier Transfer of Polymeric Carbon Nitride with Charge-Conducting  $\text{CoVO}_6\cdot 2\text{H}_2\text{O}$  for Photocatalytic  $\text{O}_2$  Evolution, *Nanomaterials.* 12 (2022) 1931. <https://doi.org/10.3390/nano12111931>.
- [98] X. Li, J. Hu, T. Yang, X. Yang, J. Qu, et al., Efficient photocatalytic  $\text{H}_2$ -evolution coupled with valuable furfural-production on exquisite 2D/2D  $\text{LaVO}_4/\text{g-C}_3\text{N}_4$  heterostructure, *Nano Energy.* 92 (2022) 106714. <https://doi.org/10.1016/j.nanoen.2021.106714>.
- [99] W. Guo, H. Luo, Z. Jiang, W. Shangguan, In-situ pressure-induced  $\text{BiVO}_4/\text{Bi}_0.6\text{Y}_0.4\text{VO}_4$  S-scheme heterojunction for enhanced photocatalytic overall water splitting activity, *Chin. J. Catal.* 43 (2022) 316–328. [https://doi.org/10.1016/S1872-0672\(21\)63846-9](https://doi.org/10.1016/S1872-0672(21)63846-9).
- [100] B. Zhang, L. Sun, G. Lei, W. Zhao, Z. Guo, et al., Effect for the electronic configurations of  $\text{LuVO}_4$  induced by  $\text{D}_{4h}$  crystal-field-splitting discovered in the systematic DFT investigation on photocatalysis capacities of vanadates, *Mater. Today Chem.* 29 (2023) 101395. <https://doi.org/10.1016/j.mtchem.2023.101395>.
- [101] K.K. Mandari, N. Son, T. Kim, M. Kang, Highly efficient  $\text{SnS}_2/\text{Ag}/\text{AgVO}_3$  heterostructures for improved charge carriers in photocatalytic  $\text{H}_2$  production, *J. Alloys Compd.* 927 (2022) 166886. <https://doi.org/10.1016/j.jallcom.2022.166886>.
- [102] X.-P. Wang, Z. Jin, X. Li, Monoclinic  $\beta\text{-AgVO}_3$  coupled with  $\text{CdS}$  formed a 1D/1D p-n heterojunction for efficient photocatalytic hydrogen evolution, *Rare Met.* 42 (2023) 1494–1507. <https://doi.org/10.1007/s12598-022-02183-y>.
- [103] A. Chowdhury, S. Balu, T.C.-K. Yang, Construction of  $\alpha\text{-Fe}_2\text{O}_3\text{-NPs}/\text{AgVO}_3\text{-NRs}$  Z-scheme heterojunction: An efficient photo(electro)catalyst for  $\text{Cr(VI)}$  reduction and oxygen evolution reactions under visible-light, *J. Environ. Chem. Eng.* 11 (2023) 109769. <https://doi.org/10.1016/j.jece.2023.109769>.
- [104] X. Wei, S. Naraginti, X. Yang, X. Xu, J. Li, et al., A novel magnetic  $\text{AgVO}_3/\text{rGO}/\text{CuFe}_2\text{O}_4$  hybrid catalyst for efficient hydrogen evolution and photocatalytic degradation, *Environ. Res.* 229 (2023) 115948. <https://doi.org/10.1016/j.envres.2023.115948>.
- [105] M.F.R. Samsudin, S. Sufian, B.H. Hameed, Epigrammatic progress and perspective on the photocatalytic properties of  $\text{BiVO}_4$ -based photocatalyst in photocatalytic water treatment technology: A review, *J. Mol. Liq.* 268 (2018) 438–459. <https://doi.org/10.1016/j.molliq.2018.07.051>.
- [106] X. Li, H. Sun, Y. Xie, Y. Liang, X. Gong, et al., Principles, synthesis and applications of dual Z-scheme photocatalysts, *Coord. Chem. Rev.* 467 (2022) 214596. <https://doi.org/10.1016/j.ccr.2022.214596>.
- [107] H. Li, L. Wang, X. Pi, M. Ma, X. Jiang, et al., Effect of the wettability of  $\text{Ag}_2\text{MoO}_4/\text{BiVO}_4$  {010} composite on the photocatalytic degradation for 17 $\alpha$ -ethinyl estradiol, *J. Alloys Compd.* 899 (2022) 163295. <https://doi.org/10.1016/j.jallcom.2021.163295>.

- [108] M.H.T. Tung, L.M. Cuong, T.T.T. Phuong, C.V. Hoang, T.T.T. Hien, et al., Construction of Ag decorated on InVO<sub>4</sub>/g-C<sub>3</sub>N<sub>4</sub> for novel photocatalytic degradation of residual antibiotics, *J. Solid State Chem.* 305 (2022) 122643. <https://doi.org/10.1016/j.jssc.2021.122643>.
- [109] D.V. Thuan, T.L. Nguyen, H. Ha, N.T. Thanh, S. Ghotekar, et al., Development of Indium vanadate and Silver deposited on graphitic carbon nitride ternary heterojunction for advanced photocatalytic degradation of residual antibiotics in aqueous environment, *Opt. Mater.* 123 (2022) 111885. <https://doi.org/10.1016/j.optmat.2021.111885>.
- [110] S. Li, S. Hu, W. Jiang, Y. Liu, Y. Liu, et al., Ag<sub>3</sub>VO<sub>4</sub> Nanoparticles Decorated Bi<sub>2</sub>O<sub>2</sub>CO<sub>3</sub> Micro-Flowers: An Efficient Visible-Light-Driven Photocatalyst for the Removal of Toxic Contaminants, *Front. Chem.* 6 (2018) 255. <https://doi.org/10.3389/fchem.2018.00255>.
- [111] D. Jiang, P. Xiao, L. Shao, D. Li, RGO-Promoted All-Solid-State g-C<sub>3</sub>N<sub>4</sub>/BiVO<sub>4</sub> Z-Scheme Heterostructure with Enhanced Photocatalytic Activity toward the Degradation of Antibiotics, *Ind. Eng. Chem. Res.* 56 (2017) 8823–8832. <https://doi.org/10.1021/acs.iecr.7b01840>.
- [112] E.S. Alsolami, I.A. Mkhali, A. Shawky, M.A. Hussein, AgVO<sub>3</sub>-anchored 2D CeO<sub>2</sub> nanocrystals prepared by solution process for visible-light-driven photooxidation of ciprofloxacin antibiotic in water, *J. Photochem. Photobiol. A: Chem.* 441 (2023) 114725. <https://doi.org/10.1016/j.jphotochem.2023.114725>.
- [113] A. Raja, N. Son, M. Kang, Reduced graphene oxide decorated transition metal manganese vanadium oxide nanorods for electrochemical supercapacitors and photocatalytic degradation of pollutants in water, *J. Taiwan Inst. Chem. Eng.* 144 (2023) 104762. <https://doi.org/10.1016/j.jtice.2023.104762>.
- [114] Z. Bao, Z. Li, Y. Du, M. Zhang, J. Wang, et al., A Solid-State Carrier Transport-Prompted Z-Scheme BiVO<sub>4</sub> Quantum Dots-Based Photocatalyst for Boosted Photocatalytic Degradation of Antibiotics, *Energy Technol.* 10 (2022) 2200536. <https://doi.org/10.1002/ente.202200536>.
- [115] P. Akhter, I. Shafiq, F. Ali, F. Hassan, R. Rehman, et al., Montmorillonite-Supported BiVO<sub>4</sub> nanocomposite: Synthesis, interface characteristics and enhanced photocatalytic activity for Dye-contaminated wastewater, *J. Ind. Eng. Chem.* 123 (2023) 238–247. <https://doi.org/10.1016/j.jiec.2023.03.039>.
- [116] A. Hassani, S. Krishnan, J. Scaria, P. Eghbali, P.V. Nidheesh, Z-scheme photocatalysts for visible-light-driven pollutants degradation: A review on recent advancements, *Curr. Opin. Solid State Mater. Sci.* 25 (2021) 100941. <https://doi.org/10.1016/j.cossms.2021.100941>.
- [117] P.J. Mafa, M.E. Malefane, A.O. Idris, B.B. Mamba, D. Liu, et al., Cobalt oxide/copper bismuth oxide/samarium vanadate (Co<sub>3</sub>O<sub>4</sub>/CuBi<sub>2</sub>O<sub>4</sub>/SmVO<sub>4</sub>) dual Z-scheme heterostructured photocatalyst with high charge-transfer efficiency: Enhanced carbamazepine degradation under visible light irradiation, *J. Colloid Interface Sci.* 603 (2021) 666–684. <https://doi.org/10.1016/j.jcis.2021.06.146>.
- [118] K. Leeladevi, J. Kumar, M. Arunpandian, M. Thirupathi, E.R. Nagarajan, Investigation on photocatalytic degradation of hazardous chloramphenicol drug and amaranth dye by SmVO<sub>4</sub> decorated g-C<sub>3</sub>N<sub>4</sub> nanocomposites, *Mater. Sci. Semicond.* 123 (2021) 105563. <https://doi.org/10.1016/j.mssp.2020.105563>.
- [119] J. Chen, X. Xu, L. Feng, A. He, L. Liu, et al., One-step MOF assisted synthesis of SmVO<sub>4</sub> nanorods for photocatalytic degradation of tetracycline under visible light, *Mater. Lett.* 276 (2020) 128213. <https://doi.org/10.1016/j.matlet.2020.128213>.
- [120] Y. Chen, Y. Zhou, J. Zhang, J. Li, T. Yao, et al., Ag bridged Z-scheme AgVO<sub>3</sub>/Bi<sub>4</sub>Ti<sub>3</sub>O<sub>12</sub> heterojunction for enhanced antibiotic degradation, *J. Phys. Chem. Solids.* 161 (2022) 110428. <https://doi.org/10.1016/j.jpcs.2021.110428>.
- [121] T. Wang, J. Cai, J. Zheng, K. Fang, I. Hussain, D. Z. Husein, Facile synthesis of activated biochar/BiVO<sub>4</sub> heterojunction photocatalyst to enhance visible light efficient degradation for dye and antibiotics: applications and mechanisms, *J. Mater. Res. Technol.* 19 (2022) 5017–5036. <https://doi.org/10.1016/j.jmrt.2022.06.177>.
- [122] P.O. Oladoye, T.O. Ajiboye, E.O. Omotola, O.J. Oyewola, Methylene blue dye: Toxicity and potential elimination technology from wastewater, *Results Eng.* 16 (2022) 100678. <https://doi.org/10.1016/j.rineng.2022.100678>.
- [123] E.A. Daher, B. Riachi, J. Chamoun, C. Laberty-Robert, W. Hamd, New approach for designing wrinkled and porous ZnO thin films for photocatalytic applications, *Colloids Surf. A: Physicochem. Eng. Asp.* 658 (2023) 130628. <https://doi.org/10.1016/j.colsurfa.2022.130628>.
- [124] X. Chen, Q. Dong, S. Chen, Z. Zhang, X. Zhang, et al., Halloysite nanotubes supported BiVO<sub>4</sub>/BaSnO<sub>3</sub> p-n heterojunction photocatalysts for the enhanced degradation of methylene blue under visible light, *Colloids Surf. A: Physicochem. Eng. Asp.* 664 (2023) 131143. <https://doi.org/10.1016/j.colsurfa.2023.131143>.
- [125] A. Karami, R. Monsef, I. Waleed, H.L. Kareem, I.T. Ibrahim, M. Salavati-Niasari, Microwave synthesized erbium vanadate nano-photocatalyst: Application for enhanced degradation of contaminated water, *Int. J. Hydrog. Energy.* 48 (2023) 8499–8513. <https://doi.org/10.1016/j.ijhydene.2022.12.017>.
- [126] S. Deka, M. Bidyarani Devi, M.R. Khan, N. Keerthana, A. Venimadhav, B. Choudhury, Piezo-photocatalytic and photocatalytic bismuth vanadate nanorods with antibacterial property, *ACS Appl. Nano Mater.* 5 (2022) 10724–10734. <https://doi.org/10.1021/acsnm.2c02072>.
- [127] M. Faisal, A. Iqbal, F. Adam, R. Jothiralingam, Effect of Cu doping on the photocatalytic activity of InVO<sub>4</sub> for hazardous dye photodegradation under LED light and its mechanism, *Water Sci. Technol.* 84 (2021) 576–595. <https://doi.org/10.2166/wst.2021.244>.
- [128] S. Bansal, A. Singh, D. Poddar, P. Jain, Fabrication and photocatalytic evaluation of functionalized chitosan decorated vanadium pentoxide nano-adsorbents for water remediation, *Ceram. Int.* 49 (2023) 8871–8885. <https://doi.org/10.1016/j.ceramint.2022.11.043>.
- [129] V. Jayaraman, C. Ayappan, A. Mani, Facile preparation of bismuth vanadate-sheet/carbon nitride rod-like interface photocatalyst for efficient degradation of model organic pollutant under direct sunlight irradiation, *Chemosphere.* 287 (2022) 132055. <https://doi.org/10.1016/j.chemosphere.2021.132055>.
- [130] K. Wannakan, K. Khansamrit, T. Senasu, S. Nanan, Ultrasound-Assisted Synthesis of a ZnO/BiVO<sub>4</sub> S-Scheme Heterojunction Photocatalyst for Degradation of the Reactive Red 141 Dye and Oxytetracycline Antibiotic, *ACS Omega.* 8 (2023) 4835–4852. <https://doi.org/10.1021/acsomega.2c07020>.
- [131] L.N. Ramavathu, B.N. Tumma, P. Justin, Photocatalytic degradation studies of malachite green dye by hydrothermally synthesized Cobalt Vanadate nanoparticles, *Int. J. Nano Dimens.* 14 (2022) 145–156. <https://doi.org/10.22034/IJND.2022.1965246.2172>.
- [132] P.K. Panda, D. Pradhan, S.K. Dash, Solar light induced photocatalytic degradation of malachite green using BiVO<sub>4</sub> catalyst, *NeuroQuantology.* 20 (2022) 1518–1526. <https://doi.org/10.48047/NQ.2022.20.20.NQ109154>.
- [133] D. Channei, P. Thammaacheep, S. Kerdphon, P. Jannoey, W. Khanitchaidecha, A. Nakaruk, Domestic microwave-assisted synthesis of Pd doped-BiVO<sub>4</sub> photocatalysts, *Inorg. Chem. Commun.* 150 (2023) 110478. <https://doi.org/10.1016/j.inoche.2023.110478>.
- [134] S.P. Keerthana, R. Yuvakkumar, P.S. Kumar, G. Ravi, D. Velauthapillai, Surfactant induced copper vanadate (β-Cu<sub>2</sub>V<sub>2</sub>O<sub>7</sub>, Cu<sub>3</sub>V<sub>2</sub>O<sub>8</sub>) for different textile dyes degradation, *Environ. Res.* 211 (2022) 112964. <https://doi.org/10.1016/j.envres.2022.112964>.
- [135] D. Vaya, P.K. Surolia, Semiconductor based photocatalytic degradation of pesticides: An overview, *Environ. Technol. Innov.* 20 (2020) 101128. <https://doi.org/10.1016/j.eti.2020.101128>.

- [136] M. Piao, Y. Sun, Y. Wang, H. Teng, Preparation of BiVO<sub>4</sub>/RGO-TNT Nanomaterials for Efficient and Recyclable Photocatalysis of Imidacloprid Insecticide, *Chem. Select.* 7 (2022) e202200182. <https://doi.org/10.1002/slct.202200182>.
- [137] H. Chawla, S. Grag, J. Rohilla, Á. Szamosvölgyi, A. Efremova, et al., Visible LED-light driven photocatalytic degradation of organochlorine pesticides (2,4-D & 2,4-DP) by Curcuma longa mediated bismuth vanadate, *J. Clean. Prod.* 367 (2022) 132923. <https://doi.org/10.1016/j.jclepro.2022.132923>.
- [138] Q. Wang, B. Xue, M. Tan, N. Li, H. Zhou, et al., Visible-light-driven Ag<sub>3</sub>VO<sub>4</sub>-BiVO<sub>4</sub>/C<sub>3</sub>N<sub>4</sub> with continuous type II heterojunctions for effective removal of Cr(VI), *J. Environ. Chem. Eng.* 11 (2023) 109245. <https://doi.org/10.1016/j.jece.2022.109245>.
- [139] H. Sun, Q. Dai, J. Liu, T. Zhou, M. Chen, et al., BiVO<sub>4</sub>-Deposited MIL-101-NH<sub>2</sub> for Efficient Photocatalytic Elimination of Cr(VI), *Molecules.* 28 (2023) 1218. <https://doi.org/10.3390/molecules28031218>.
- [140] L.-H. Wang, H.-Y. Zeng, J. Xiong, S. Xu, D.-S. An, BiVO<sub>4</sub>/PANI composite with p-n heterostructure for enhanced photocatalytic activity towards Cr(VI) reduction, *Vacuum.* 202 (2022) 111203. <https://doi.org/10.1016/j.vacuum.2022.111203>.
- [141] G. Xu, M. Du, J. Zhang, T. Li, Y. Guan, C. Guo, Facile fabrication of magnetically recyclable Fe<sub>3</sub>O<sub>4</sub>/BiVO<sub>4</sub>/CuS heterojunction photocatalyst for boosting simultaneous Cr(VI) reduction and methylene blue degradation under visible light, *J. Alloys Compd.* 895 (2022) 162631. <https://doi.org/10.1016/j.jallcom.2021.162631>.
- [142] P. Liu, J. Yi, R. Bao, H. Zhao, Theory-oriented Synthesis of 2D/2D BiVO<sub>4</sub>/MXene Heterojunction for Simultaneous Removal of Hexavalent Chromium and Methylene Blue, *ChemCatChem.* 13 (2021) 3046. <https://doi.org/10.1002/cctc.202100315>.
- [143] S. Luo, S. Li, S. Zhang, Z. Cheng, T.T. Nguyen, M. Guo, Visible-light-driven Z-scheme protonated g-C<sub>3</sub>N<sub>4</sub>/wood flour biochar/BiVO<sub>4</sub> photocatalyst with biochar as charge-transfer channel for enhanced RhB degradation and Cr(VI) reduction, *Sci. Total Environ.* 806 (2022) 150662. <https://doi.org/10.1016/j.scitotenv.2021.150662>.
- [144] V. Balakumar, C. Chuaicham, K. Sasaki, K. Sekar, Fabrication of BiVO<sub>4</sub>/ reduced graphene oxide photocatalyst for hexavalent chromium reduction under visible region, *Mater. Today.* 50 (2022) 400–405. <https://doi.org/10.1016/j.matpr.2021.11.381>.
- [145] U. Zahoor, M.I. Rameel, A.H. Javed, M. Abdullah Khan, J.Y. Al-Humaidi, et al., Yttrium Doped Bismuth Vanadate Titania Heterojunction for Efficient Photoreduction of Cr from Wastewater Under Visible Light, *Int. J. Environ. Res.* 26 (2022) 88. <https://doi.org/10.1007/s41742-022-00466-x>.
- [146] J. Sun, Y. Rong, Y. Hou, L. Tu, Q. Wang, et al., Synchronous removal of tetracycline and copper (II) over Z-scheme BiVO<sub>4</sub>/rGO/g-C<sub>3</sub>N<sub>4</sub> photocatalyst under visible-light irradiation, *Environ. Sci. Pollut. Res.* 29 (2022) 19148–19164. <https://doi.org/10.1007/s11356-021-16996-4>.
- [147] M. Alhaddad, M.S. Amin, Z.I. Zaki, Novel BiVO<sub>4</sub>/ZnO heterojunction for amended photoreduction of mercury (II) ions, *Opt. Mater.* 127 (2022) 112251. <https://doi.org/10.1016/j.optmat.2022.112251>.
- [148] X. Hu, R. Guo, X. Chena, Z. Bi, J. Wang, W. Pan, Bismuth-based Z-scheme structure for photocatalytic CO<sub>2</sub> reduction: A review, *J. Environ. Chem. Eng.* 10 (2022) 108582. <https://doi.org/10.1016/j.jece.2022.108582>.
- [149] A. Bhattacharya, A. Selvaraj, Photocatalytic conversion of CO<sub>2</sub> into beneficial fuels and chemicals – a new horizon in atmospheric CO<sub>2</sub> mitigation, *Process Saf. Environ. Prot.* 156 (2021) 256–287. <https://doi.org/10.1016/j.psep.2021.10.003>.
- [150] K. Zhao, X. Liu, Q. He, W. Zhou, K. Yang, et al., Preparation and characterization of Sm<sup>3+</sup>/Tm<sup>3+</sup> co-doped BiVO<sub>4</sub> micro-squares and their photocatalytic performance for CO<sub>2</sub> reduction, *J. Taiwan Inst. Chem. Eng.* 144 (2023) 104737. <https://doi.org/10.1016/j.jtice.2023.104737>.
- [151] J. Li, W. Shao, M. Geng, S. Wan, M. Ou, Y. Chen, Combined Schottky junction and doping effect in CdxZn1-xS@Au/BiVO<sub>4</sub> Z-Scheme photocatalyst with boosted carriers charge separation for CO<sub>2</sub> reduction by H<sub>2</sub>O, *J. Colloid Interface Sci.* 606 (2022) 1469–1476. <https://doi.org/10.1016/j.jcis.2021.08.103>.
- [152] J. Wei, S. Zhang, J. Sun, T. Liang, Z. Li, et al., Z-scheme CoAl-layered double hydroxide/indium vanadate heterojunction for enhanced and highly selective photocatalytic reduction of carbon dioxide to carbon monoxide, *J. Colloid Interface Sci.* 629 (2023) 92–102. <https://doi.org/10.1016/j.jcis.2022.08.148>.
- [153] M. Yu, J. Wang, G. Li, S. Zhang, Q. Zhong, Construction of 3D/2D indium vanadate /graphite carbon nitride with nitrogen defects Z-scheme heterojunction for improving photocatalytic carbon dioxide reduction, *J. Mater. Sci. Technol.* 154 (2023) 129–139. <https://doi.org/10.1016/j.jmst.2022.12.070>.
- [154] J. Li, F. Wei, Z. Xiu, X. Han, Direct Z-scheme charge transfer of Bi<sub>2</sub>WO<sub>6</sub>/InVO<sub>4</sub> interface for efficient photocatalytic CO<sub>2</sub> reduction, *Chem. Eng. J.* 446 (2022) 137129. <https://doi.org/10.1016/j.cej.2022.137129>.
- [155] F. Mei, K. Dai, J. Zhang, L. Li, C. Liang, Ultrathin indium vanadate/cadmium selenide-amine step-scheme heterojunction with interfacial chemical bonding for promotion of visible-light-driven carbon dioxide reduction, *J. Colloid Interface Sci.* 608 (2022) 1846–1856. <https://doi.org/10.1016/j.jcis.2021.10.034>.
- [156] L. Wang, D. Chen, S. Miao, F. Chen, C. Guo, et al., Nitric acid-assisted growth of InVO<sub>4</sub> nanobelts on protonated ultrathin C<sub>3</sub>N<sub>4</sub> nanosheets as an S-scheme photocatalyst with tunable oxygen vacancies for boosting CO<sub>2</sub> conversion, *Chem. Eng. J.* 434 (2022) 133867. <https://doi.org/10.1016/j.cej.2021.133867>.
- [157] S. Gong, X. Teng, Y. Niu, X. Liu, M. Xu, et al., Construction of S-scheme 0D/2D heterostructures for enhanced visible-light-driven CO<sub>2</sub> reduction, *Appl. Catal. B.* 298 (2021) 120521. <https://doi.org/10.1016/j.apcatb.2021.120521>.
- [158] A. Akhoondi, M. Mirzaei, M.Y. Nassar, Z. Sabaghian, F. Hatami, M. Yusuf, New strategies in the preparation of binary g-C<sub>3</sub>N<sub>4</sub>/MXene composites for visible-light-driven photocatalytic applications, *Synth. Sinter.* 2 (2022) 151–169. <https://doi.org/10.53063/synsint.2022.24121>.
- [159] M. Khazaei, M. Arai, T. Sasaki, C.-Y. Chung, N.S. Venkataramanan, et al., Novel electronic and magnetic properties of two-dimensional transition metal carbides and nitrides, *Adv. Funct. Mater.* 23 (2013) 2185–2192. <https://doi.org/10.1002/adfm.201202502>.
- [160] L. Li, Y. Yang, L. Yang, X. Wang, Y. Zhou, Z. Zou, 3D hydrangea-like InVO<sub>4</sub>/Ti<sub>3</sub>C<sub>2</sub>T<sub>x</sub> hierarchical heterosystem collaborating with 2D/2D interface interaction for enhanced photocatalytic CO<sub>2</sub> reduction, *Chem. Nano. Mat.* 7 (2021) 815–823. <https://doi.org/10.1002/cnma.202100100>.
- [161] A. Bafaqeer, M. Tahir, N.A.S. Amin, N. Al-Bastaki, A. Hamood, H.A. Thabit, Performance analysis of externally reflected photoreactor for CO<sub>2</sub> conversion to methanol using f-C<sub>3</sub>N<sub>4</sub>/ZnV<sub>2</sub>O<sub>6</sub> S-scheme photocatalyst, *Environ. Technol. Innov.* 30 (2023) 103032. <https://doi.org/10.1016/j.eti.2023.103032>.
- [162] L. Zhang, J. Zhang, H. Yu, J. Yu, Emerging S-Scheme Photocatalyst, *Adv. Mater.* 34 (2022) 2107668. <https://doi.org/10.1002/adma.202107668>.
- [163] S. Li, N. Hasan, H. Ma, G. Zhu, L. Pan, et al., Hierarchical V<sub>2</sub>O<sub>5</sub>/ZnV<sub>2</sub>O<sub>6</sub> nanosheets photocatalyst for CO<sub>2</sub> reduction to solar fuels, *Chem. Eng. J.* 430 (2022) 132863. <https://doi.org/10.1016/j.cej.2021.132863>.